SEARCH COIL MAGNETOMETERS FOR THE ISTP POLAR AND WIND SPACECRAFT

by

George Blair Hospodarsky

A thesis submitted in partial fulfillment
of the requirements for the Master
of Science degree in Physics
in the Graduate College of
The University of Iowa

May 1992

Thesis supervisor: Professor Donald A. Gurnett

Graduate College
The University of Iowa
Iowa City, Iowa

CERTIFICATE OF APPROVAL

MASTER'S THESIS

This is to certify that the Master's thesis of

George Blair Hospodarsky

has been approved by the Examining Committee for the thesis requirement for the Master of Science degree in Physics at the May 1992 graduation.

Thesis committee: Donald A. Gurnett
Thesis supervisor

Edward R. McCluskey
Member

Robert J. Merlino
Member

ACKNOWLEDGEMENTS

I wish to express my sincere appreciation to Professor Don Gurnett for allowing me the opportunity to work on this project, and for his valuable help and guidance. There are few opportunities for graduate students to work on the design and construction of spaceflight hardware today, and I appreciate the chance to do so. I would also like to thank Bill Schintler and Miles Bailey for their work on the new preamplifier, and their patience and understanding for my many stupid questions. Don Kirchner, Steve Remington, Dan Odem, Pete Sheyko, Bob Barrie, and the rest of the Plasma Wave Team also deserve a special thank you. It is impossible to build successful instruments without a good team, and we have one here at Iowa.

A special thanks goes to Kathy Kurth and Tricia Becker for typing the many revisions of the thesis. Without them, I would still be pecking away at the keyboard. I would also like to thank Mark DeBower, Bob Beall, and Joyce Chrisinger for many of the figures in the thesis. I thank Marilyn and Karen for making sure I had the proper paperwork in on time to allow me to graduate.

I also would like to thank my many friends that have made graduate school enjoyable, and continue to do so, especially Tami, Karen, Chris, Robin and Lucy, Bill, Lee, Rick, Glen, Billy-Bob, Kevin, Jim and Jim, Tak, Jerry, Jeff, and the many others that I have forgotten to mention. Lastly I wish to thank my family, especially the

Curleys, who were always there when I needed a break away from the Physics building, and my mom and brothers, who have supported and encouraged me through this long process we call higher education.

This research was supported in part by NASA contract NAS5-30371 through Goddard Space Flight Center, by the University of Iowa Graduate College, and by the Iowa Space Grant Consortium through the National Space Grant Fellowship Program.

ABSTRACT

Low frequency electromagnetic waves play an important role in the dynamic processes that occur in space plasmas. Search coil magnetometers are one of the primary tools used in the study of the magnetic component of these low frequency electromagnetic waves. The small size, mass, and power consumption of search coil magnetometers make them ideal for spaceflight operations. This thesis describes the ISTP Polar and Wind search coil magnetometers currently being constructed at the University of Iowa. The basic theory of search coil magnetometers is presented. Specific design considerations and improvements of the Polar and Wind search coils over earlier designs are discussed. A description of the calibration methods for the Polar and Wind search coils is given, and possible improvements for future search coil magnetometers are suggested.

TABLE OF CONTENTS

LIST OF TABLES

LIST OF FIGURES

CHAPTER I. INTRODUCTION

Most of the matter in our Universe is in the form of an ionized gas called a plasma. Electric and magnetic fields play a fundamental role in the dynamic processes that occur in space plasmas. The measurement and study of electric and magnetic fields is essential for a complete understanding of the dynamics and evolution of plasmas. Magnetometers are one of the primary tools employed in the measurement of the magnetic fields in space plasmas. Several types of magnetometers have been used for measurements of magnetic fields in space plasmas. Generally, there are two types of magnetometers; those that can measure static fields, and those that can measure time varying fields. The primary types of static field magnetometers are the fluxgate magnetometer, which uses the nonlinear properties of magnetic materials to sense static fields, the helium vapor magnetometer, which uses the light transmission properties of helium, and the alkali vapor magnetometer, which uses the Zeeman effect. Magnetometers for sensing time-varying magnetic fields are based on the Faraday induction effect. The primary types of time-varying magnetometers are the loop magnetometer, which uses a simple conducting loop to sense time varying magnetic fields, and the search coil magnetometer, which uses a ferromagnetic rod inserted through a coil with a large number of turns of conducting wire.

The first magnetometer flown in space was a fluxgate magnetometer carried on the Soviet Sputnik 3 spacecraft which was launched in May 1958. The first U.S. magnetometer was a search coil magnetometer flown on Pioneer 1 in October 1958. These early magnetometers were designed to measure the Earth's and the Moon's magnetic field, and had upper frequency limits of only a few hertz. The first magnetometer flown on a spacecraft that was designed to measure naturally occurring plasma wave magnetic fields was a loop magnetometer launched in 1962 on the University of Iowa designed spacecraft Injun 3. The Injun 3 loop magnetometer had a frequency bandwidth of approximately 500 to 7000 Hz and was specifically designed to measure very-low-frequency (VLF) electromagnetic waves. The first University of Iowa search coil magnetometer was flown on the Explorer 50 (IMP J) spacecraft, which was launched in 1973. Since then, search coil magnetometers built at the University of Iowa have also flown on the Hawkeye 1, ISEE 1, ISEE 2, ISEE 3, DE 1, PDP and CRRES spacecraft.

This thesis will discuss the design and development of an advanced search coil magnetometer that is to be flown on the Polar and Wind spacecraft. The Polar and Wind spacecraft are part of the NASA International Solar-Terrestrial Physics Project (ISTP). The ISTP program is an international program that is made up of a large number of spacecraft which will allow plasma and plasma wave measurements in the Earth's magnetosphere and in the solar wind. The U.S. part of this program consists of the Polar and Wind spacecraft. Studies of global mechanisms for mass, momentum,

and energy flow through geospace plasmas will be possible with these spacecraft. The Polar spacecraft is currently scheduled to be launched in 1994, and will be placed in a highly eccentric polar orbit around the Earth. The Wind spacecraft is scheduled to be launched in 1993, and will be placed in a small halo orbit around the L1 Earth-Sun Lagrangian point. This orbit will allow the solar wind to be studied upstream from the Earth, thereby providing the upstream conditions required for studying the interaction of the solar wind with the Earth's magnetosphere.

Search coil magnetometers are very important in the study of very-low-frequency electromagnetic waves in space plasmas. Their small size, mass, and power consumption, coupled with their good frequency range and noise level, make them ideal for space flight applications. The basic configuration of a search coil magnetometer consists of many thousands of turns of wire wound on a high permeability core as shown in Figure 1. The output of the coil is usually connected to a preamplifier, which amplifies the induced voltage and conditions the signal for transmission to the main electronics package. Search coil magnetometers are usually used in conjunction with electric antennas to measure electromagnetic plasma waves, both natural occurring waves and waves generated by ground transmitters. One of the primary uses of search coil magnetometers is to determine if a wave is electrostatic or electromagnetic. They are also used for determining the wave normal, the polarization, and the Poynting vector.

Search coil magnetometers are used to study many different wave phenomena in space plasmas. Figure 2 lists some of these phenomena, and shows their typical frequencies and magnetic field amplitudes. The curved line is the noise level of the ISEE 1 and 2 search coils, which were built at the University of Iowa, and launched in 1977. The Polar and Wind search coil magnetometers have an advanced design that provides lower noise levels and improved sensitivity, allowing even weaker signals to be measured.

CHAPTER II. BASIC PRINCIPLES

The basic operating principle of a search coil magnetometer is Faraday's law of magnetic induction. This law states that a loop of wire with a time-varying magnetic field passing through it will have a time-varying voltage induced across it that is proportional to the time rate of change of the magnetic field. This law can be written as

$$V = -C\frac{d}{dt}[\vec{B}\cdot\hat{n}] \tag{1}$$

where C is a constant that depends on the area of the loop and on the properties of the core material, $\vec{B}$ is the magnetic field vector, and $\hat{n}$ is a unit vector along the axis of the coil. Expanding the derivative, taking into account the possible motion of the coil and considering both temporal and spatial variations of the field, it can be shown that

$$V = -C[\vec{B}\cdot\frac{d\hat{n}}{dt} + \hat{n}\cdot\frac{d\vec{B}}{dt} + \vec{u}\cdot\nabla[\vec{B}\cdot\hat{n}]] \quad . \tag{2}$$

The first term represents the voltage induced by the angular motion of the coil. The second term represents the voltage induced by explicit time variations of the magnetic field. This term is the one we are most interested in, as it represents the magnetic component of electromagnetic waves. The third term represents the voltage induced by convective motions of the coil with velocity $\vec{u}$ relative to the magnetic field $\vec{B}$. This

third term includes the voltage induced by the search coil moving through a magnetic field gradient. In most space environments, the first and third terms are negligible or can be filtered out, and the second term dominates.

The induced voltage for a search coil magnetometer that has a solenoidal coil of N turns of wire enclosing a ferromagnetic core can be written

$$V = -NA\mu_e\left(\frac{dB}{dt}\right) \quad , \tag{3}$$

where A is the cross-sectional area of the core, μ_e is the effective permeability of the core, and (dB/dt) is the time variation of the magnetic field component parallel to the coil axis. If the variation of the magnetic field is sinusoidal, this equation reduces to

$$V = -2\pi NA\mu_e f B_o \times 10^{-7} \mu V \tag{4}$$

where B_o is the amplitude of the magnetic signal in nT, A is in cm^2, and f is the frequency of the time variation. This expression can be simplified, and is usually written

$$V = -KfB_o \ \mu V \tag{5}$$

where K is defined as the coil constant of the search coil and is given by

$$K = 2\pi NA\mu_e \times 10^{-7} \ \frac{\mu V}{nT\ Hz} \quad . \tag{6}$$

The above analysis assumed that a search coil magnetometer is a pure inductor, but search coil magnetometers also have a resistance, due to the resistance of the wire,

and a capacitance, due to the self capacitance between the turns in the coil. These additional properties can be modeled using the equivalent circuit shown in Figure 3. The voltage induced by a time varying magnetic field is represented by a voltage source in series with an inductor, labeled L. The resistance of the wire, modeled by the resistor labeled R_1, is in series with the inductor. The resistor R_1 also accounts for any losses due to eddy currents, hysteresis, skin effects, and proximity to nearby conductors. In most cases, these losses are much smaller than the loss due to the resistance of the wire, and these losses can be neglected. The self capacitance, modeled by the capacitor labeled C, is parallel to L and R_1. The self capacitance is due to a potential difference between adjacent turns and layers of the coil. The resistor labeled R_D is called the damping resistor. This resistor controls the sharpness of the resonant peak, and accounts for the input impedance of the preamplifier. An analysis of the circuit shows that Equation 5 is modified to

$$V = \frac{-KfB_o}{\sqrt{(1+\frac{R_1}{R_D}-\omega^2LC)^2+(\frac{\omega L}{R_D}+\omega CR_1)^2}} \quad \mu V \tag{7}$$

where $\omega = 2\pi f$. For typical values of L, C, R_1, and R_D, the denominator is ≈ 1, for ω below $\omega_r = 1/\sqrt{LC}$, where $f_r = \omega_r/2\pi$ is called the resonant frequency. The resonant frequency is the frequency which produces the largest induced voltage. For frequencies near ω_r, the denominator may be much less than 1, depending on the exact values of L, C, R_1, and R_D. For frequencies well above the resonant frequency, Equation 7 is

no longer valid, as secondary capacitances and other effects start to become important. These higher order effects are difficult to model, and may change a great deal with temperature, and over time. Because of these second order effects, search coil magnetometers are usually designed with resonant frequencies above the frequency range they are expected to measure.

Another important characteristic of the equivalent circuit is its impedance. The real part of the impedance determines the thermal noise (also called Johnson noise) voltage produced by the search coil. The noise voltage must be small to allow the measurement of weak magnetic fields. The real part of the impedance of the circuit in Figure 3 is

$$Z_r = \frac{R_1(1+\frac{R_1}{R_D}-\omega^2LC)+\omega L(\frac{\omega L}{R_D}+\omega CR_1)}{(1+\frac{R_1}{R_D}-\omega^2LC)^2+(\frac{\omega L}{R_D}+\omega CR_1)^2} \; ohms \quad . \tag{8}$$

An analysis of this equation shows that the real part of the impedance ranges from $\approx R_1$ ohms at low frequencies, to $\approx R_D$ ohms near the resonant frequency. The Johnson noise voltage of a search coil over a frequency bandwidth Δf, is given by Robinson [1974] as

$$\frac{V_{Johnson}}{\sqrt{\Delta f}} = \sqrt{4k_B T Z_r} \quad \frac{Volts}{\sqrt{Hz}} \tag{9}$$

where k_B is Boltzmann constant, T is the temperature in degrees Kelvin, and Z_r is the real part of the impedance defined in Equation 8. The Johnson noise will be discussed in more detail later.

The noise voltage is needed to determine one of the most important characteristics of a search coil, its noise level. The noise level is defined as the magnetic signal strength that induces a voltage equal to the noise voltage. Setting the noise level, Equation 9, equal to the output voltage, Equation 7, and solving for the magnetic signal, we find

$$\frac{B_N}{\sqrt{\Delta f}} = \frac{\sqrt{4k_B T(R_1 + \frac{R_1^2}{R_D} + \frac{\omega^2 L^2}{R_D})}}{Kf} \quad \frac{nT}{\sqrt{Hz}} \tag{10}$$

The noise level is usually squared,

$$\frac{B_N^2}{\Delta f} = \frac{4k_B T}{K^2 f^2}(R_1 + \frac{R_1^2}{R_D} + \frac{\omega^2 L^2}{R_D}) \quad \frac{nT^2}{Hz} \tag{11}$$

which has units of magnetic field spectral density. The noise level determines the minimum magnetic signal a search coil magnetometer can measure over a given frequency bandwidth. Analyzing Equation 11 for typical values of L, C, R_1, and R_D, $R_1 \ll R_D$, $R_1^2/R_D \ll R_1$, and $L^2/R_D \ll R_1$, we find

$$\frac{B_N^2}{\Delta f} \simeq \frac{4k_BT}{(NA\mu_e \times 10^{-7})^2} \left(\frac{R_1}{\omega^2} + \frac{L^2}{R_D}\right) \frac{nT^2}{Hz} \quad . \tag{12}$$

At low frequencies R_1/ω^2 determines the noise level, but at higher frequencies L^2/R_D sets a lower limit. This equation does not include the noise voltage of the preamplifier. Including the preamplifier noise voltage in Equation 11, the noise level becomes

$$\frac{B_N^2}{\Delta f} = \frac{4k_BT(R_1 + \frac{R_1^2}{R_D} + \frac{\omega^2L^2}{R_D})}{(Kf)^2} + \frac{(n_{amp}^2/\Delta f)}{(Kf)^2} \left[(1 + \frac{R_1}{R_D} - \omega^2LC)^2 + \right. \tag{13}$$

$$\left. \left(\frac{\omega L}{R_D} + \omega CR_1\right)^2\right] \frac{nT^2}{Hz}$$

where $n_{amp}^2/\Delta f$ is the noise spectral density of the preamplifier. Analyzing Equation 13 for typical values of L, C, R_1, and R_D, we find

$$\frac{B_N^2}{\Delta f} \simeq \frac{4k_BT}{(NA\mu_e \times 10^{-7})^2} \left(\frac{R_1}{\omega^2} + \frac{L^2}{R_D}\right) + \frac{(n_{amp}^2/\Delta f)}{(NA\mu_e \times 10^{-7})^2} \left(\frac{1}{\omega^2}\right) \frac{nT^2}{Hz} \quad . \tag{14}$$

This equation shows that the noise of the preamplifier can play an important role in the noise level of a search coil magnetometer, especially at low frequencies. A good search coil magnetometer design uses the optimum combination of the above variables to obtain the lowest noise level possible in the frequency range of interest.

CHAPTER III. DESIGN CONSIDERATIONS

Effective Permeability

The effective permeability of the core is needed to determine the sensitivity of the search coil from Equation 4. Magnetic materials are rated according to their permeability, μ_i, where permeability is defined as the ratio of the magnetic flux density in the material to the ambient magnetic field density in the absence of the material. For the analysis of a laminated bar or rod, the more significant parameter is the effective permeability, μ_e. The effective permeability of long rods constructed of high permeability materials is less than the closed-loop permeability by which ferromagnetic materials are rated [Bozorth and Chapin, 1942]. The effective permeability is determined by the length to diameter, ℓ/d, ratio of the rod. Hayashi [1988] gives for $\mu_i \gg 1$, and $\ell \gg$ d

$$\mu_e = \frac{1}{D_B(1 - \frac{1}{\mu_i}) + \frac{1}{\mu_i}} \tag{15}$$

where μ_i is the closed-loop permeability of the material and D_B is the demagnetizing factor determined from

$$D_B = \frac{\ell n(\frac{3}{2}\frac{\ell}{d}) - 1}{(\frac{\ell}{d})^2} \quad . \tag{16}$$

It should be noted that both μ_i and μ_e are dimensionless constants. This equation gives the theoretical value of μ_e at the center of the rod, but the effective permeability is known to decrease near the ends of the rods [Bozorth and Chapin, 1942]. Hill [1962] gives μ_e as a function of distance from the center of the rod

$$\mu_e = \mu_1(1 - F\frac{x^2}{\ell^2}) \tag{17}$$

where μ_1 is the effective permeability at the mid-point of the core determined from Equation 15, x is the distance from the center of the core, ℓ is the length of the core, and F is a dimensionless constant that specifies the permeability near the end of the core. Hill states that F=3.6.

The effective permeability in Equation 4 is defined as the effective permeability at the position of the turns of wire. Equation 17 shows that the largest effective permeability is achieved for coils located near the center of the core. Equation 15 also shows that a larger ℓ/d ratio produces a larger μ_e. However, the effective permeability for large ℓ/d ratios ($\gtrsim$ 100) is sensitive to temperature changes and mechanical stresses. Also, there are size and weight limits for search coil magnetometers designed for space applications which restrict the ℓ/d ratio.

Resistance of the Wire

Underhill [1910] gives for the resistance of the wire of a search coil with a square bobbin

$$R = 4(a + 0.7854T)N\rho \text{ ohms} \tag{18}$$

where a is the width of the bobbin, T is the depth of the windings, ρ is the resistance per unit length, and N is the number of turns. The type of wire and the diameter of the wire determine ρ. For a given number of turns, the depth of the windings, T, will also depend on the diameter of the wire. From Equations 12 and 14, we can see that the resistance of the wire should be kept as small as possible in order to minimize the noise level of the search coil. This minimization is accomplished by choosing the largest diameter wire that will fit on the bobbin for a given number of turns.

Inductance

The inductance of a solenoid on a high permeability core can be estimated from the following formula [Parady, 1974]

$$L = \frac{\mu_0 \mu_e N^2 A}{\ell} \tag{19}$$

where μ_0 is the permeability constant, μ_e is the effective permeability of the core, A is the cross-sectional area of the core in square meters, N is the number of turns, and ℓ is the length of the core in meters. It should be noted that the inductance varies with the square of the number of turns and is proportional to μ_e. As the resonant frequency

is proportional to the inverse of the square root of the inductance, the resonant frequency is proportional to the inverse of the number of turns and also to the inverse of the square root of μ_e. This relationship leads to a trade off as more turns leads to a better sensitivity, but decreases the bandwidth of the search coil.

Capacitance

The capacitance of a solenoid is difficult to model, as the method of winding the solenoid has a large effect on the final capacitance. Also, capacitance from the wires connecting the bobbin to the preamplifier, or in the preamplifier itself can also play a large role. An estimate for the capacitance of one section of a multi-section coil is given by Hill [1962]

$$C = \frac{0.00381\,\pi\, r_1\, \epsilon_r\, W}{(K_1 - 1) d\, \lambda} \qquad pF \tag{20}$$

where r_1 is the mean radius of the coil, W is the width of the coil, ϵ_r is the average dielectric constant of the insulation on the wire, K_1 is the ratio of the distance between the center of two adjacent wires and the diameter of the wire, d is the diameter of the wire, and λ is the number of layers of wire.

Equation 7 shows that for a large resonant frequency, it is desirable for the capacitance to be as small as possible. One way to accomplish a lower capacitance is to split the coil into sections. If a coil that originally had a capacitance C, is split into n sections, each section would have a capacitance C/n. These sections are connected in series, which gives a new capacitance of C/n^2 for the whole search coil. There is

also a capacitance between the sections, which when taken into account, gives a total capacitance of

$$C_{tot} = \frac{C}{n^2} + \frac{C_1}{(n-1)} \tag{21}$$

where C_1 is the capacitance between adjacent sections. As we want C_{tot} to be smaller than the original capacitance, C_1 should be kept small. This reduction in the capacitance is accomplished by having a space between the sections. There is a limit to the effectiveness of splitting the coils. If n is small, C_{tot} varies inversely to n^2, but as n becomes large, the $C_1/(n-1)$ term starts to dominate. Another limitation is that the resistance of the wire increases as the number of sections are increased, which raises the noise level of the searce coil as seen from Equation 11. There is also a size limit on a search coil to be flown in space, which limits both the number of sections, and the space between each section.

Damping Resistor

The damping resistor plays an important role in the sensitivity and noise level of the search coil as shown in Equations 7 and 13. The damping resistor can be an actual resistor placed in parallel with the coils, the input impedance of the preamplifier, or a combination of the two.

Noise and Noise Sources

The ability for search coil magnetometers to measure weak signals is determined by the amount of noise present. Noise is the unwanted signal that obscure the desired

signal. There are various types and sources of noise. Some of the most important ones are: the Johnson noise due to the resistance of the coil, noise in the amplifier, and interference from outside sources. Johnson noise, also known as Nyquist noise or thermal noise, is the noise found in any material with a resistance. It is caused by the random motion of the free electrons in the material. This random motion produces small instantaneous potential differences between the ends of the material. Since the noise voltage is random, it has a flat frequency spectrum, and is often called "white noise." For resistors, it is usually written as

$$V_{Johnson} = \sqrt{4k_B T\, R\, \Delta f} \qquad Volts \tag{22}$$

where T is the temperature in degrees Kelvin, k_B is Boltzmann's constant, R is the resistance, and Δf is the frequency bandwidth. It is important to notice that Johnson noise depends on the square-root of the temperature. In a complex circuit the resistance R must be replaced with the real impedance Z_r of the circuit [Robinson, 1974]. This substitution gives the Johnson noise as shown in Equation 9.

The other type of noise found in a search coil magnetometer is noise from the preamplifier. This noise is usually made up of three main components, 1/f, or flicker noise, shot noise, and Johnson noise. The 1/f noise usually dominates at low frequencies, while shot and Johnson noise dominates at higher frequencies.

The 1/f noise is given its name due to the fact that it has a spectrum proportional to the inverse of the frequency. The magnitude of this noise varies markedly with the material, and also the construction of the component can have a large effect on the

noise magnitude. Resistors can exhibit this noise, along with transistors, FETs, diodes and vacuum tubes. The 1/f noise is also found in many non-electronic systems. The flow of sand in an hour glass, the flow of traffic on an expressway, and the loudness of classical music versus time all show a 1/f spectrum [Horowitz and Hill, 1980]. This dependance on the material and construction technique makes it difficult to estimate its magnitude before an actual amplifier is built.

Shot noise is due to the current not being a continuous flow, but actually made up of discrete electrical charges. This discreteness results in statistical fluctuations of the current. Horowitz and Hill [1980] gives

$$I_{shot} = \sqrt{2\ q\ I_{dc}\ \Delta f} \tag{23}$$

where q is the electric charge, I_{dc} is the dc current, and Δf is the bandwidth. For large currents, the noise current is usually a very small fraction of the original current, but for small currents, the fluctuations can become a significant fraction of the original current. Shot noise is found in solid state devices, such as transistors and diodes, where electrons randomly cross a pn junction. This effect is analogous to the noise of raindrops hitting a tin roof, which is where it gets its name. It has a flat frequency response like Johnson noise, and in a circuit, it may be difficult to distinguish which of the two is the major noise source at the output.

The total noise voltage of a search coil magnetometer with no outside signals present, is given by

$$n_{total} = \sqrt{(n_{coil}G)^2 + (n_{amp})^2} \quad (24)$$

where n_{coil} is the noise voltage due to the coil from Equation 9, G is the gain of the amplifier, and n_{amp} is the noise voltage due to the amplifier.

The other type of noise important in search coil magnetometers flown on spacecraft is interference. This noise includes interference during testing and calibration, and interference from other instruments on the spacecraft while operating in space.

The interference most often encountered in the lab with a search coil magnetometer is 60 Hz interference from the power lines. Other sources of interference are from computer monitors, usually in the tens of kHz range, and signals from radio stations, 800 kHz and above. This interference must be reduced or removed to get a good calibration of the instrument. The actual noise voltage of the search coil magnetometer can only be found if this interference is removed. This problem is discussed in more detail in the calibration section.

Electrical interference from the spacecraft also increases the noise level, as it obscures the natural signals the instrument is trying to measure. Figure 4 shows an example of interference from the Galileo spacecraft. A complex spectrum of interference can be observed between 100 Hz and 1000 Hz. This interference makes it difficult to measure any natural signals in this frequency range. Various steps can and should be taken to reduce magnetic interference. Magnetometers should be deployed as far from the spacecraft body as possible. Most interference fields are

dipole in nature. Dipole magnetic fields vary as $1/r^3$, where r is the distance between the noise source and the sensor. If r is large, then the interference will be reduced, hopefully below the noise level of the search coil. For this reason, search coil magnetometers are often mounted on the end of a boom, far from the spacecraft electrical systems. Current carrying wires should be twisted pairs, and large current loops in the spacecraft harness design should be avoided. Any current loops that are necessary should be made as small as possible to minimize the magnetic moment, AI. Power converters should operate at the highest possible frequency, preferably above the frequency range of the sensor. Shielding can reduce magnetic interference, but due to weight considerations, shielding can only be applied to small components. At spacecraft testing and calibration, each instrument should be tested individually with the magnetometers to examine its possibility for generating interference.

CHAPTER IV. POLAR AND WIND SEARCH COILS

The Polar and Wind search coils are the first search coils built at The University of Iowa to use preamplifiers constructed with surface mount technology. The new preamplifiers improve the sensitivity and noise level of the search coil magnetometers over earlier University of Iowa search coil designs. Figure 5 shows an outline drawing of the search coils. The main components are the housing that contains and protects the electronics, a high permeability core, two bobbins containing thousands of turns of wire each, and a preamplifier located in the center section of the housing. Each component will be discussed in more detail below.

Housings

The housing of the Polar and Wind search coils are shown in Figure 6. They are constructed of Vespel and were coated at Goddard Space Flight Center with vacuum deposited aluminum and silver conductive paint to provide a electrostatic shield, and then painted with black paint to provide the proper thermal properties.

Core and Bobbins

The core of the Polar and Wind search coils was purchased from the Arnold Engineering Company and consists of a 4 mil supermalloy laminated bar with dimensions of 3/16 x 3/16 x 15.5 inches. It has an initial permeability, μ_i, of 60,000 at 100 Hz. The ℓ/d ratio of 82.7 and μ_i = 60,000 gives an effective permeability at

the center of the rod of 1738 (see Equation 15). For the Polar and Wind search coils, the bobbins are positioned 1.275 inches from the center of the core as shown in Figure 7. The bobbins were machined from Delrin and are shown in Figure 8. There are eight sections containing the wire, seven of which contain the primary windings, and one that contains a calibration winding as shown in Figure 9. The Polar search coils contains 1430 turns of #40 AWG wire per section for the primary winding, for a total of 10,010 turns per bobbin. The Wind search coils contains 5715 turns of #44 AWG wire per section for a total of 40,005 turns per bobbin. Both the Polar and Wind search coils contain a calibration winding of 1000 turns of #40 AWG wire in the eighth section.

The variation of μ_e over the length of the core coupled with the location of the bobbins on the core causes a reduction in the effective permeability determined above. This correction factor of the effective permeability was determined by finding μ_e for the center of each section of primary winding from Equation 17. The average of the correction factors of the seven sections was determined and this average was multiplied by the value 1738 determined from Equation 15 for the center of the core. The average correction factor was found to be 0.876, which gives a corrected effective permeability of 1522.

The effects of the position of the bobbins on the core was examined with the Polar engineering model search coil. The effective permeability was determined from Equation 17 for each position of the bobbins on the core. Figure 10 shows the

variation of output voltage of one side of the preamplifier with the effective permeability. As can be seen, the curve is approximately a straight line, as expected from the linear relation of output voltage to μ_e from Equation 4. Figure 11 shows the variation of the inductance of the two bobbins with the effective permeability. These curves are also approximately straight lines, as expected from the linear relation of L and μ_e from Equation 19. These small deviations from a straight line are probably due to Equation 17 losing some accuracy near the ends of the core. The difference in the inductance between the two bobbins is probably due to the bobbins having a different number of turns. This hypothesis is supported by the fact that the resistance of bobbin 1 is 1136 ohms and bobbin 2 is 1260 ohms.

The effective permeability at the center of the core was calculated from these induction measurements by rewriting Equation 19 as

$$\mu_e = \frac{L\,\ell}{f\,A\,N^2\mu_0} \tag{25}$$

where ℓ is the length of the core in meters, L is the measured inductance in Henrys, N the number of turns (assumed to be 10,010), A is the area of the core in square meters, μ_0 is the permeability constant, and f is the correction factor of μ_e for the position of the bobbin on the core. This equation gives $\mu_e = 2375$ for bobbin 1, and $\mu_e = 2760$ for bobbin 2. These values are much larger than the value of 1738 obtained from Equation 15. This discrepancy will be discussed in the next section.

Resistance, Inductance, and Capacitance

The resistance, inductance, and capacitance of the Polar and Wind search coils were measured on a HP 4192A LF Impedance Analyzer. The results and the theoretical predictions from Equations 18, 19, and 20 are shown in Table 1. As can be seen, the theoretical and measured values do not agree. This discrepancy in the capacitance is not unexpected due to the previously mentioned difficulties of modeling the self capacitance of a multilayered coils. There are also capacitance effects present from the leads coming off the bobbins which were not considered in Equation 20. It was observed that moving the leads could cause a small ($<10\%$) change in the measured capacitance. The measured inductance was found to be $\approx 35\%$ larger than the predicted value. The Japanese Geotail search coil's inductance [Hayashi, 1988], was also compared to the theoretical value predicted from Equation 19, and was also found to be $\approx 35\%$ too large. The difference between the theoretical and the experimental value may be due to the length term, ℓ in the denominator of Equation 19. Pasahow [1985] states that ℓ is the magnetic path length of the core. Since the permeability of the core decreases near the ends, it would be reasonable to assume that the magnetic path length is smaller than the actual core length.

The theoretical and measured resistances of the Polar and Wind search coils agree reasonably well. The small difference is probably due to difficulties in determining the depth of the windings and the exact width of the bobbin which are needed in Equation 18 to determine the theoretical resistance.

Preamplifiers

The Polar and Wind search coil preamplifiers are a new design. They were the first search coil preamplifiers to be built using surface mount technology at the University of Iowa. A circuit built using surface mount technology occupies less volume than the same circuit built using the old cordwood mounting technique. This reduction in size allowed the new, more advance preamplifier to be built, without increasing the size or weight of the search coils. Figure 12 shows a schematic of the Polar search coil preamplifier. The amplifier design is the same for the Polar and Wind search coils except for the resistors R2 and R26. These resistors control the value of the input impedance of the amplifier, which determines the damping resistance. Figure 13 shows a simplified block diagram of the amplifier. For a differential signal across the inputs, the amplifier acts like two separate amplifiers as shown in Figure 14.

The separation into two amplifiers allows the coils to be isolated from each other, which for a fixed resonance frequency permits the number of turns on each bobbin to be doubled. This doubling of the number of turns increases the sensitivity of the search coil by a factor of two, but keeps the same frequency bandwidth as a single coil with half as many turns.

The net effect is a $\sqrt{2}$ improvement in the signal-to-noise ratio. To see this improvement, note that the noise voltage out of each side of the preamplifier adds as

$$n_{amp} = \sqrt{V_n^2 + V_n^2} = \sqrt{2}\,V_n \qquad \frac{Volts}{\sqrt{Hz}} \tag{26}$$

where V_n is the noise voltage of one side of the preamplifier. This equation assumes that the noise is the same on both outputs. The noise level improvement due to the new amplifier can be determined from

$$\frac{B_N}{\sqrt{\Delta f}} = \frac{\sqrt{2}\ V_n}{2V_{out}} = \frac{V_n}{\sqrt{2}\ V_{out}}\ \frac{nT}{\sqrt{Hz}} \tag{27}$$

where V_{out} is the voltage out of each side of the preamplifier. This amplifier design gives a $\sqrt{2}$ improvement of the noise level with the same bandwidth compared to a search coil with the old preamplifiers. In theory, one could continue this process with n preamplifiers, which would give you a $\sqrt{n}$ improvement. Of course, there is a limit to the size, weight, and power that can be allocated to a search coil that is to be flown on a spacecraft which would limit n.

The gain of the amplifier can be found from Figure 14 to be

$$G = \frac{A(11{,}999)}{499A + (11{,}999)} \tag{28}$$

where A is the open loop gain. The open loop gain of the Wind search coil amplifiers were measured and found to be ≈ 70, which gives a gain ≈ 18. This value of the gain agrees very well with measured sensitivities of the Wind search coils.

Polar Search Coils

The Polar search coils have 10,010 turns of #40 AWG wire on each bobbin, for a total of 20,020 turns. The coil constant, K, from Equation 6 is approximately 3.9 μV/(nT Hz). Taking into account a preamplifier gain of 18, we have a total sensitivity of ≈ 70 μV/(nT Hz). The resonant frequency is approximately 10,000 Hz. The

resistance of the wire is approximately 1250 ohms, which gives a noise voltage of 4.55 $nV/\sqrt{Hz}$ at 300° K. The new preamplifier design increased the sensitivity by a factor of two compared to the ISEE 1 and 2 search coils, which had coil plus amplifier sensitivity of $\approx 35\ \mu V/(nT\ Hz)$, and a resonant frequency of 10,000 Hz [Gurnett et al., 1978]. The transfer function of the Polar prototype search coil and the theoretical prediction from Equation 7 are shown in Figure 15. The values used to determine the theoretical curve were

$$\begin{aligned} R_1 &= 1250\ \Omega \\ R_D &= 2.25\ M\ \Omega \\ L &= 17\ H \\ C &= 10.3\ pF \\ N &= 20{,}020 \\ \mu_e &= 1522 \\ G &= 18 \end{aligned} \qquad (29)$$

The noise level of the Polar prototype search coil was measured in the lab by the μ-metal shield method. Figure 16 compares the Polar measured noise level with the ISEE 1 and 2 noise levels [Gurnett and Anderson, 1978]. As can be seen, above 800 Hz the Polar noise level is approximately $\sqrt{2}$ times lower than the ISEE noise levels as expected from the new amplifier design. Below 800 Hz, the higher noise level of the Polar search coil is probably caused by interference signals, mostly 60 Hz, and its

harmonics. A noise voltage calibration will be done with the flight units at a low noise site to determine the actual noise level at these lower frequencies. The flight Polar search coils are currently being constructed, with completion scheduled for June, 1992.

Wind Search Coils

The Wind search coils are similar to the Polar search coils but are optimized for lower frequencies. They consists of 40,005 turns of #44 AWG wire on each bobbin for a total of 80,010 turns. The resistance of the wire on each bobbin is approximately 12,850 ohms. This resistance gives a noise voltage of 14.6 nV/$\sqrt{\text{Hz}}$ at 300° K. The coil constant from Equation 6 is approximately 16.0 μV/(nT Hz). The total coil constant taking into account an amplifier gain of 18 is approximately 288 μV/(nT Hz). The resonant frequency is $\approx$1600 Hz. This resonant frequency is much lower than predicted by Equation 7 for the measure capacitance and inductance of the bobbins (see Table 1). The deviation from the theoretical value is due to a stray capacitive coupling on the flight preamplifier boards. Figure 17 shows the transfer function of the Wind spare search coil and the theoretical curve from Equation 7 with an added capacitance to correct for the stray capacitance. The values used for the theoretical calculation were

$$
\begin{aligned}
R_1 &= 12{,}850 && \Omega \\
R_D &= 4.535 && M\,\Omega \\
L &= 280 && H \\
C &= 34.26 && pF \\
N &= 80{,}010 \\
\mu_e &= 1522 \\
G &= 17.74
\end{aligned}
\qquad (30)
$$

Figure 18 compares the noise level of the Wind spare search coil measured at a low noise field site and the ISEE 3 search coil inflight noise levels [Gurnett and Anderson, 1978]. These two search coils have the same number of total turns, 80,010, so their noise levels should be similar. The Wind search coils have a higher resonant frequency which gives them a lower noise level at higher frequencies.

The Wind flight search coils have been constructed, tested, calibrated, and delivered to the University of Minnesota for integration with their plasma wave instrument. Figure 19 shows a photograph of the Wind B_z search coil magnetometer.

CHAPTER V. CALIBRATION

The sensitivity of the Polar and Wind search coil magnetometers are calibrated by two different methods. They both involved applying a sinusoidal magnetic field of a known frequency, phase, and magnitude, and measuring the search coil's output frequency, phase, and voltage. The first method employs a transmitting loop to produce the applied magnetic field. The second method employs a shielded solenoid to produce the applied magnetic field. Sixty Hertz interference from power lines, and other low frequency emissions, primarily from computers, are easily detected by the search coil magnetometers, and can often saturate the preamplifier. This interference must be reduced or eliminated to obtain accurate calibrations.

The transmitting loop method involves driving a triangular transmitting loop with a known current and frequency at a known distance from the search coil. The magnetic field produced by the loop at the search coil location can be calculated exactly since the current and the geometry and are known. Figure 20 shows a typical setup of this method. The search coil is placed at a distance L from the center of a triangular transmitting loop, and a height h from the bottom of the loop as shown. The axis of the search coil is perpendicular to the plane of the transmitting loop. The voltage across the eight ohm resistor is measured to determine the current, I, in the transmitting loop. The

magnetic field produced by the transmitting loop at the search coil is determined from this current for a given L, d, and h from

$$|\vec{B}| = \frac{N\mu_o I}{4\pi}[\frac{1}{r_1}(\cos\alpha_1 - \cos B_1) - \frac{1}{r_2}(\cos\alpha_2 - \cos B_2) + \frac{1}{r_3}(\cos\alpha_3 - \cos B_3)] \quad Tesla \tag{31}$$

where

$$r_1 = h$$

$$r_2 = D_3 \sin\alpha_2$$

$$r_3 = D_3 \sin B_3$$

$$\alpha_1 = \cos^{-1}(\frac{L + \frac{d}{2}}{D_1})$$

$$\alpha_2 = 1.0472 - \cos^{-1}(\frac{L}{D_3})$$

$$\alpha_3 = 1.0472 - \alpha_1$$

$$B_1 = \cos^{-1}(\frac{L - \frac{d}{2}}{D_2})$$

$$B_2 = 1.0472 + B_1$$

$$B_3 = 2.094395 - \alpha_2$$

$$D_1 = [(L + \frac{d}{2})^2 + h^2]^{1/2}$$

$$D_2 = [(L - \frac{d}{2})^2 + h^2]^{1/2}$$

$$D_3 = [(0.866\ d - h)^2 + L^2]^{1/2}$$

and N is the number of turns of the transmitting loop. Substituting I=V/R, R=8 ohms, N=8 turns, and V equal to the voltage measured across the resistor, we find

$$|\vec{B}| = \frac{N\ V}{R} \times 10^{-7}\ C(L,\ d,\ h) = V \times 10^{-7}\ C(L,\ d,\ h)\ \ Tesla \qquad (32)$$

where C(L,d,h) is the term from Equation 31 that depends on L, d, and h.

The transmitting loop method must be performed away from low frequency interference sources, such as 60 Hz interference from power lines, and also away from magnetic materials, such as steel beams or metal lab benches. Magnetic materials distort the applied field, causing an error in the calibration. This distortion can be observed in Figure 21, which shows the measured coil constant, K, of the Wind spare search coil using the transmitting loop method in the lab. The curves are for distances of L=5 feet and L=8 feet. If there was no distortion present, the two curves would be identical, as was observed when the test was repeated at a low noise field site. It is believed that the steel beams in the floor and ceiling caused the distortion. No magnetic shield room exists at the University of Iowa so the transmitting loop calibration must be performed

at a field site if an accurate calibration is required. This method gives a very accurate magnitude and phase calibration. The main drawback with the method is that accurate calibrations cannot be obtained in the lab. Weather limits when field calibration may be attempted, as rain and snow may damage the test equipment and the search coils. Cleanliness and static protection are also difficult to control in the field.

The shielded solenoid method involves placing the search coil in the center of a long solenoid. A known current is applied to the solenoid, which produces the magnetic field. The solenoid consist of ten turns of wire with a radius of 13 cm. Each turn is separated by 6.7 cm, with a total length of the solenoid of 60.3 cm. The equivalent circuit of the solenoid is shown in Figure 22. The magnetic field produced at the center of the solenoid by each individual coil can be determined from the following formula:

$$B(z) = \frac{\mu_0 I}{2}\left(\frac{r^2}{(z^2 + r^2)^{3/2}}\right) \quad Tesla \tag{33}$$

where r is the radius of the coil, I is the current in each turn, and z is the distance from the coil to center of the solenoid. Summing over all ten turns of the solenoid, and substituting I=V/R, we find for the center of the solenoid

$$B = \frac{\mu_0 V}{2(5000)}(28.02) = 3.52\times10^{-9}\ V \quad Tesla \tag{34}$$

where V is the voltage measured across the 50 ohm resistor.

To reduce the interference signals, the solenoid is enclosed in a μ-metal shield. The magnetic shielding allows calibration measurements to be performed in the lab. The

current μ-metal shield reduces the interference signals by over 60 dB. However this shielding approach has certain problems. First, in some cases the μ-metal shield does not reduce the interference signals to levels low enough to allow a good calibration. Second, the μ-metal shield changes the field characteristics of the solenoid. If the perturbation is large enough, the errors in the calibration can be excessive. Figure 23 show a comparison of the transfer function of the Wind spare search coil obtained at a low noise field site by the transmitting loop method at two distances verses the solenoid in the μ-metal shield method measured in the lab. As can be seen, the perturbation in the applied magnetic field is small, confirming that the shielded solenoid provides a good calibration technique for determining the sensitivity of the search coils.

The noise voltage of the search coil must also be measured and calibrated to determine the noise level of the search coil. This calibration is usually done in the μ-metal shield with no calibration signal present. As the μ-metal does not eliminate all the 60 Hz interference found in the lab, best results are obtained at a low noise field site. The search coil is placed in the μ-metal shield and powered by a set of batteries. The noise voltage of the search coil is then measured by a spectrum analyzer. Figure 24 shows the setup for such a noise level calibration.

The noise voltage of the Wind search coils was measured both in the lab and at a low noise field site using the solenoid in the μ-metal shield. The resulting noise levels are shown in Figure 25. As can be seen, the noise level at low frequencies is much lower when measured at a low noise field site. At higher frequencies, the noise levels are very similar.

CHAPTER VI. FUTURE WORK

Various possible design changes which may have improved the search coil magnetometers were discovered during this project, but due to time constraints in building the search coils, were not examined in detail, or implemented. These design changes should be examined before future search coils are built, and if improvements are found to exists, the changes should be implemented.

The first design change that should be implemented is to place the bobbins at the center of the core. This placement will increase the sensitivity by over 10% compared to the Polar and Wind search coils. The placement in the center of core will require the housing to be redesigned to allow a compartment for the preamplifier.

A second possible design change would be to redesign the preamplifier, specifically to lower its noise voltage. The preferred approach would be to use prefabricated chip amplifiers, whose small size would allow the coil to be split into more sections. This splitting would lower the noise level by $\sqrt{n}$ as shown in Equation 27 where n is the number of separate coils. One difficulty with prefabricated chip amplifiers is their high cost, much higher than the current preamplifiers.

Another possible design change would be to adopt a negative feedback system, as shown in Figure 26 [Hayashi, 1988]. This type of system has been flown on the Galileo spacecraft, and is to be flown on the Geotail spacecraft. The use of a feedback

winding on the core flattens the transfer function, allowing one to make the damping resistance infinite. Looking at Equation 11 for the noise level, we see that as R_d increase, the noise level decreases. Although this approach should reduce the noise level, we note that the noise levels of the Galileo and Geotail search coil magnetometers do not show a marked improvement over the Polar and Wind search coils. Future work should be done to determine if a feedback winding would improve the noise level of the present search coil magnetometer design.

One last possible design change would be to lower the temperature or use superconducting wire for the coil. This change would lower the noise level in Equation 11 since R_1 would be reduced. There would still be the noise due to the amplifier as shown in Equation 13, so the overall improvement would depend on the amplifier noise. There is also the added complication of providing a low temperature, particularly if the wire was maintained in a superconducting state.

CHAPTER VII. CONCLUSION

The Polar and Wind search coil magnetometers provide improvement over the earlier University of Iowa search coil designs. The higher sensitivity, and lower noise levels of the Polar and Wind search coils will allow weaker magnetic signals to be measured. They will provide new data for understanding the plasmas in our solar system, and for investigating the interaction of low frequency electromagnetic waves with plasmas.

REFERENCES

Bozorth, R. M., and D. M. Chapin, Demagnetizing Factors of Rods, J. Applied Phys., 13, 320, 1942.

Gurnett, D. A., and R. R. Anderson, et al., ISEE 1, ISEE 2, and ISEE 3 Plasma Wave Investigation Calibration Records, The University of Iowa, Iowa City, Iowa, 1978.

Gurnett, D. A., F. L. Scarf, R. W. Fredricks, and E. J. Smith, The ISEE-1 and ISEE-2 Plasma Wave Investigation, IEEE Trans. Geo. Elect., GE-16, 253, 1978.

Hayashi, K., Improvement of the Tri-Axial Search Coils Onboard Geotail Satellite and Electromagnetic Interference (EMI) Problem on the Satellite, Thesis, Kanazawa University, 1988.

Hill, L. K., Micropulsation Sensors with Laminated MUMETAL Cores, Thesis, The University of Texas, 1962.

Horowitz, P., and W. Hill, The Art of Electronics, Cambridge University Press, Cambridge, 1980.

Parady, B., Measurement of Low Frequency Magnetic Fluctuations in the Magnetosphere, Thesis, University of Minnesota, 1974.

Pasahow, E., Electronics Ready Reference Manual, McGraw-Hill Book Company, New York, 1985.

Robinson, F., N. H., Noise and Fluctuations in Electronic Devices and Circuits, Oxford University Press, London, 1974.

Underhill, C. R., Solenoids Electromagnets and Electromagnetic Windings, D. Van Nostrand Company, New York, 1910.

Table 1. Comparison of Theoretical and Measured Values for the Polar and Wind Search Coil

	Polar		Wind	
	Theory	Measured	Theory	Measured
Inductance (H)	11	17	176	280
Capacitance (pF)	4.5	13.8	1.22	11.3
Resistance (ohms)	1170	1250	12,967	12,800

Figure 1. A sketch of the basic configuration of a search coil magnetometer.

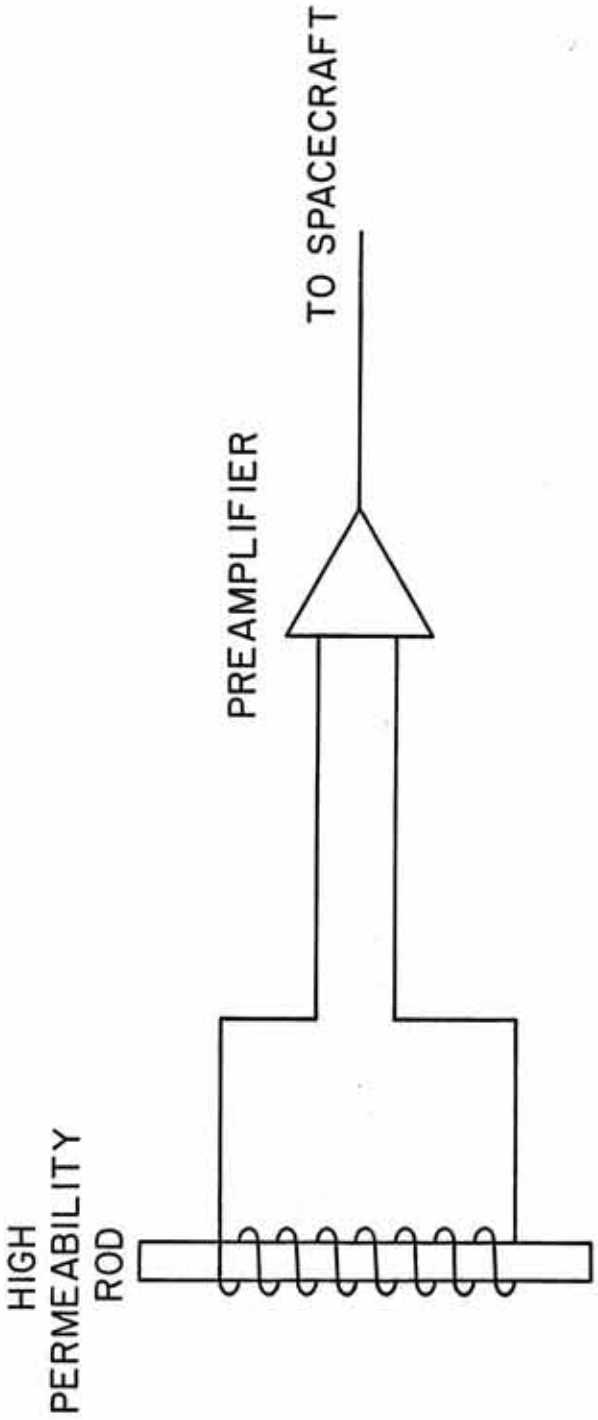
A-G92-134
TO SPACECRAFT
PREAMPLIFIER
HIGH
PERMEABILITY
ROD

Figure 2. A sketch of several space plasma phenomena, and their typical magnetic field amplitudes and frequencies. The curved line is the noise level of the ISEE 1 and 2 search coils which were constructed at the University of Iowa and launched in 1977.

A-G89-275-2

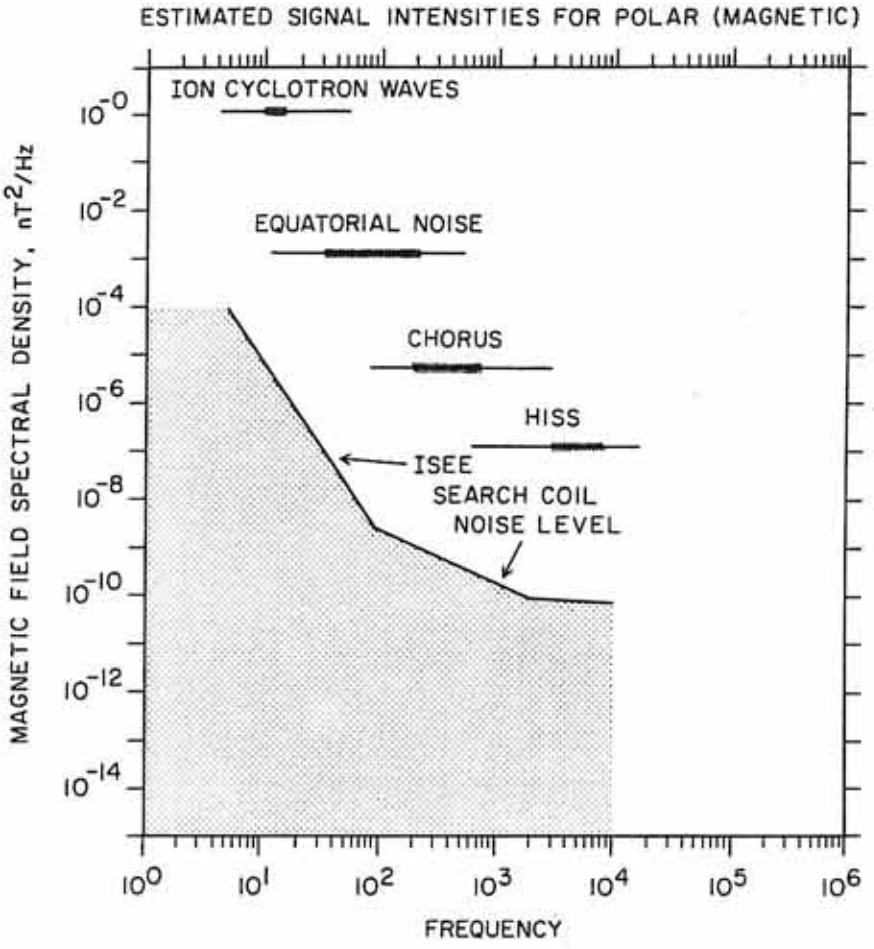
ESTIMATED SIGNAL INTENSITIES FOR POLAR (MAGNETIC)
ION CYCLOTRON WAVES
EQUATORIAL NOISE
CHORUS
HISS
ISEE
SEARCH COIL
NOISE LEVEL
MAGNETIC FIELD SPECTRAL DENSITY, nT²/Hz
10⁻⁰
10⁻²
10⁻⁴
10⁻⁶
10⁻⁸
10⁻¹⁰
10⁻¹²
10⁻¹⁴
10⁰
10¹
10²
10³
10⁴
10⁵
10⁶
FREQUENCY

Figure 3. The equivalent circuit of the search coil magnetometer.

A-G91-624

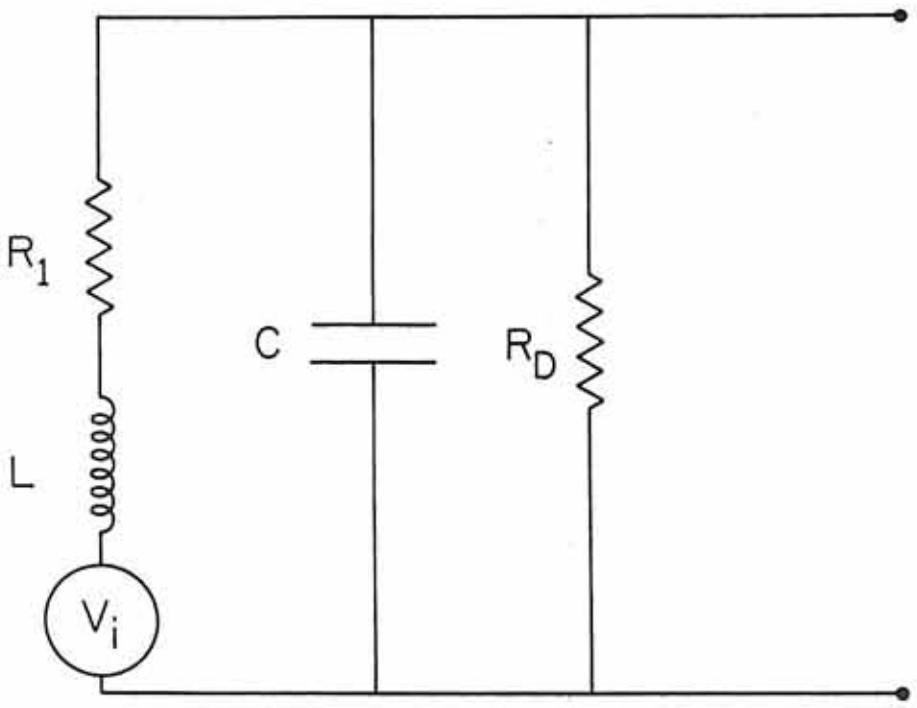

Figure 4. A spectrogram showing spacecraft-generated interference measured by the Galileo search coil magnetometer. A complex spectrum of interference is observed from below 100 Hz to about 1000 Hz.

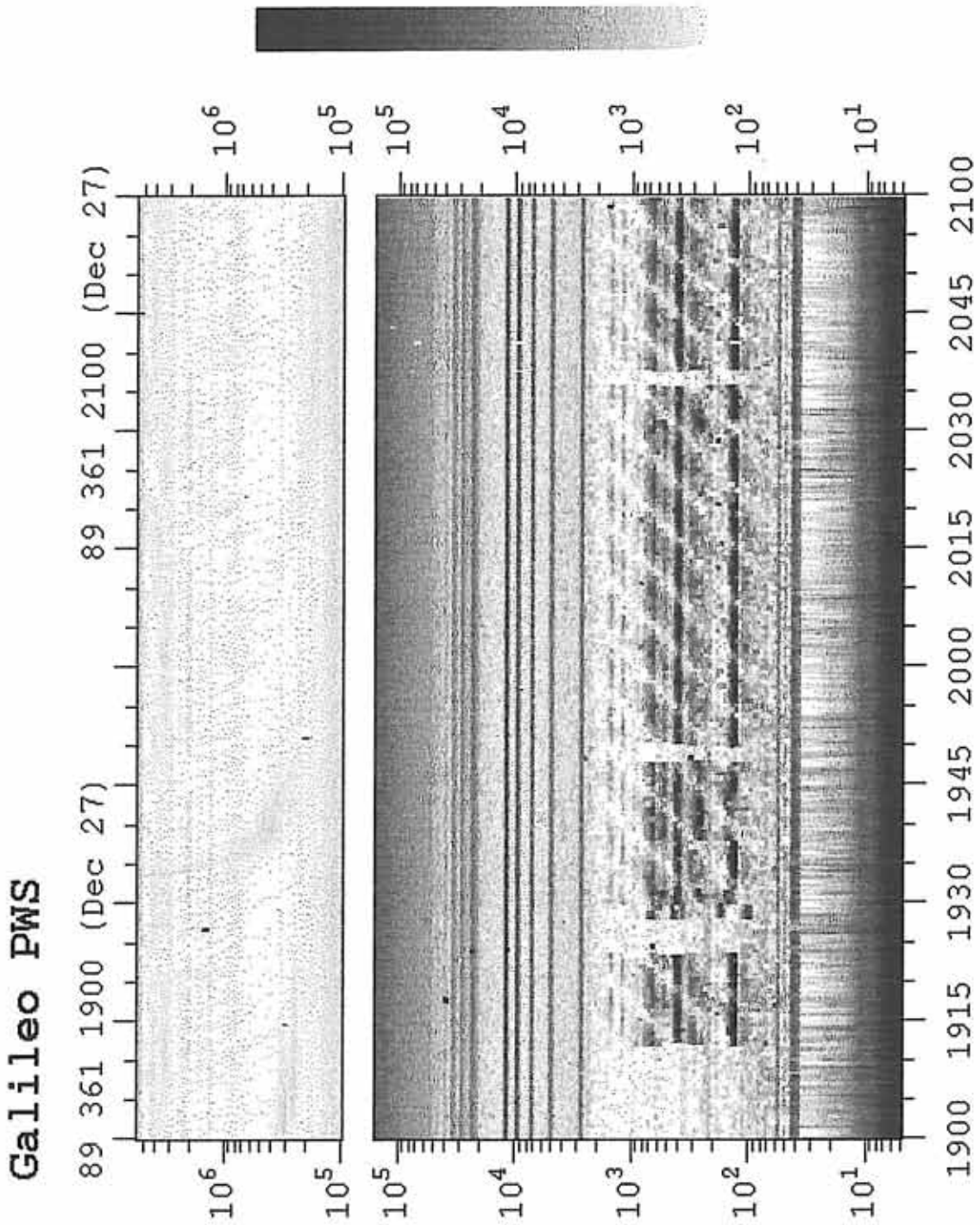
Galileo PWS
89 361 1900 (Dec 27)
89 361 2100 (Dec 27)
1900 1915 1930 1945 2000 2015 2030 2045 2100
10^6
10^5
10^5
10^4
10^3
10^2
10^1

Figure 5. A sketch of the Polar and Wind search coil magnetometer showing the main components.

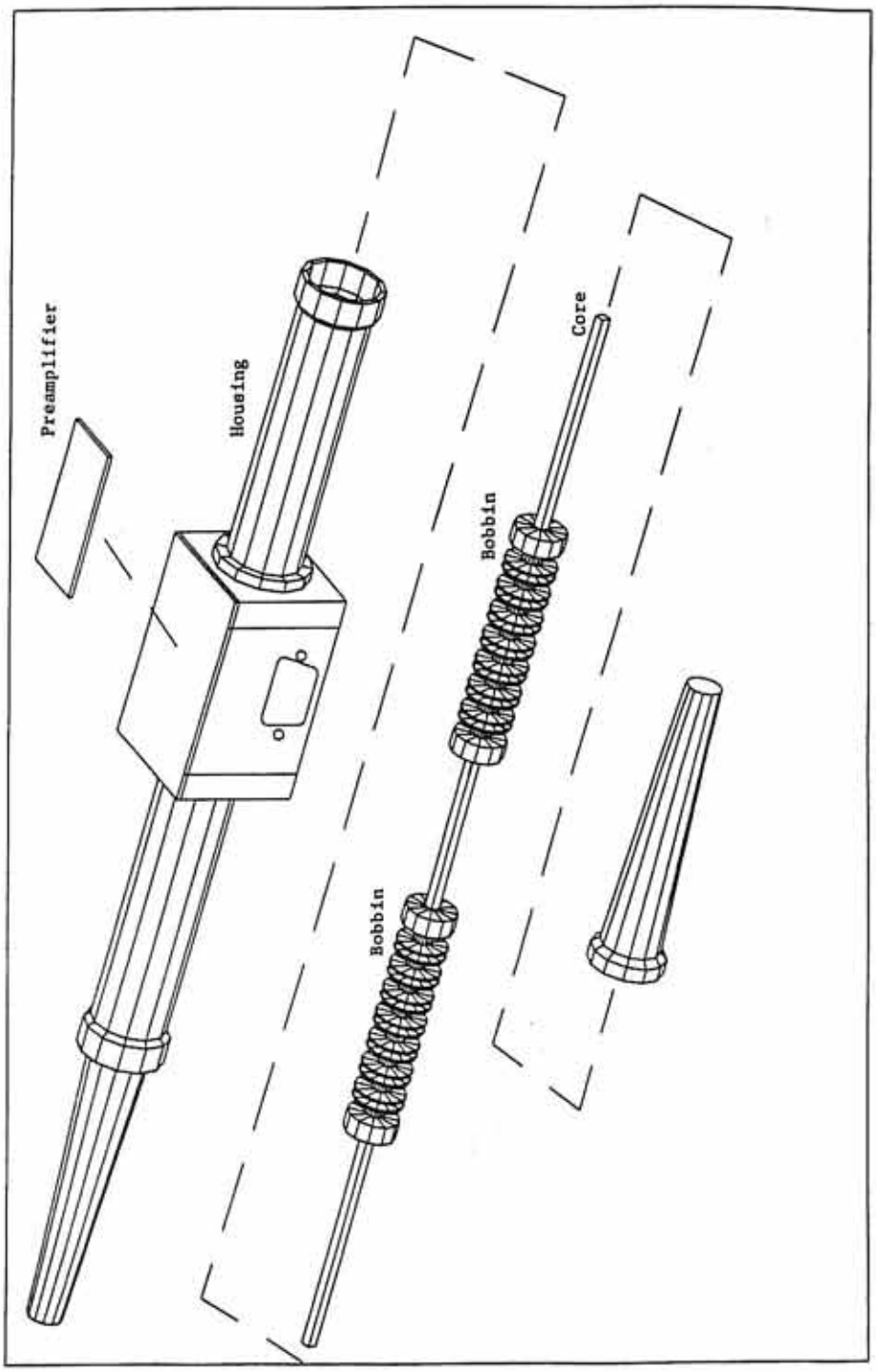
Preamplifier
Housing
Core
Bobbin
Bobbin

Figure 6. The Polar and Wind search coil magnetometer housings. The dimensions are given in inches.

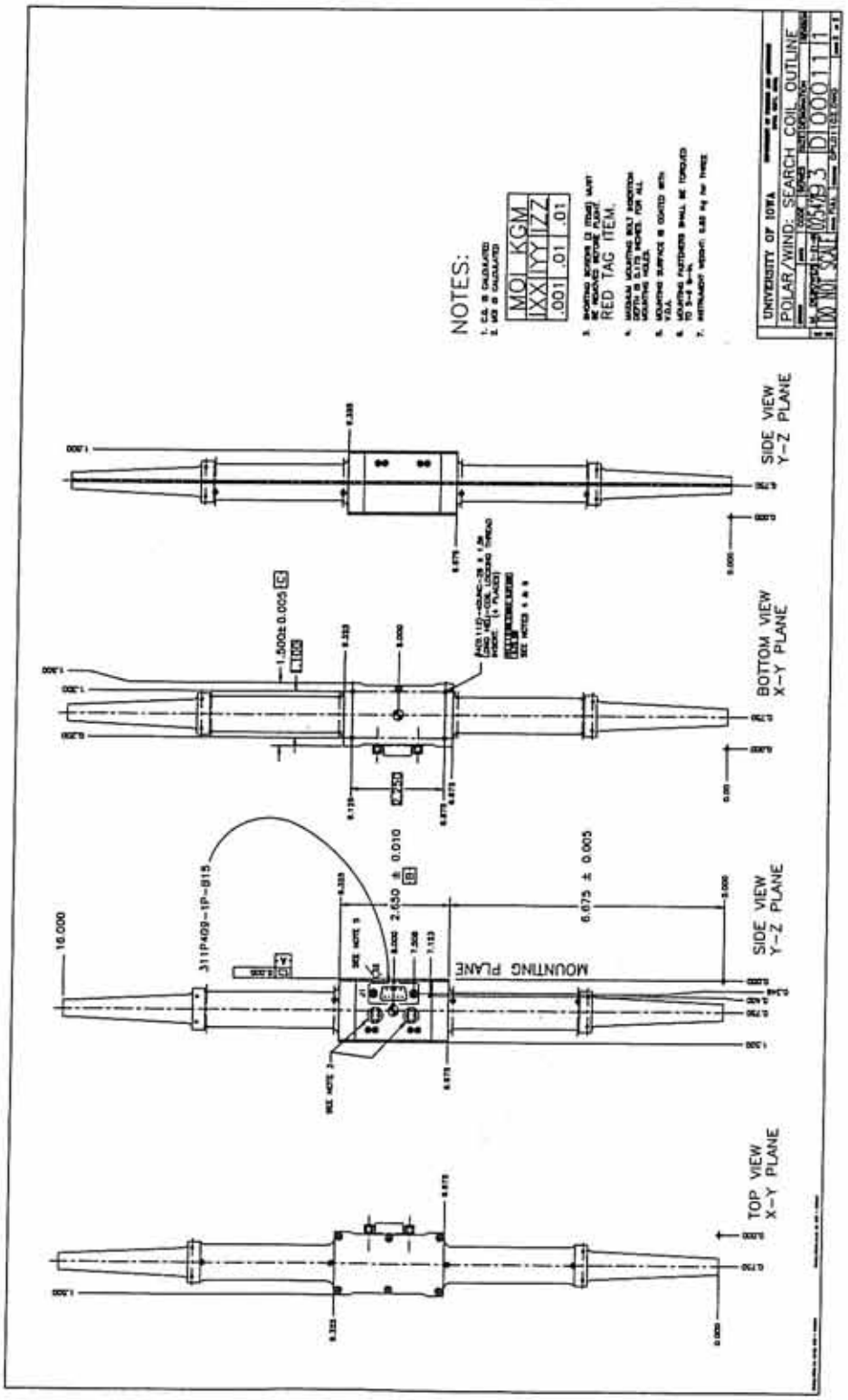
NOTES:
MOI KGM
IXX IYY IZZ
.001 .01 .01
RED TAG ITEM.
UNIVERSITY OF IOWA
POLAR/WIND: SEARCH COIL OUTLINE
SIDE VIEW Y-Z PLANE
BOTTOM VIEW X-Y PLANE
SIDE VIEW Y-Z PLANE
TOP VIEW X-Y PLANE
MOUNTING PLANE
311P409-1P-915
16.000
2.650 ± 0.010
6.675 ± 0.005
1.500±0.005

Figure 7. A sketch showing the location of the bobbins on the core. The dimensions are given in inches.

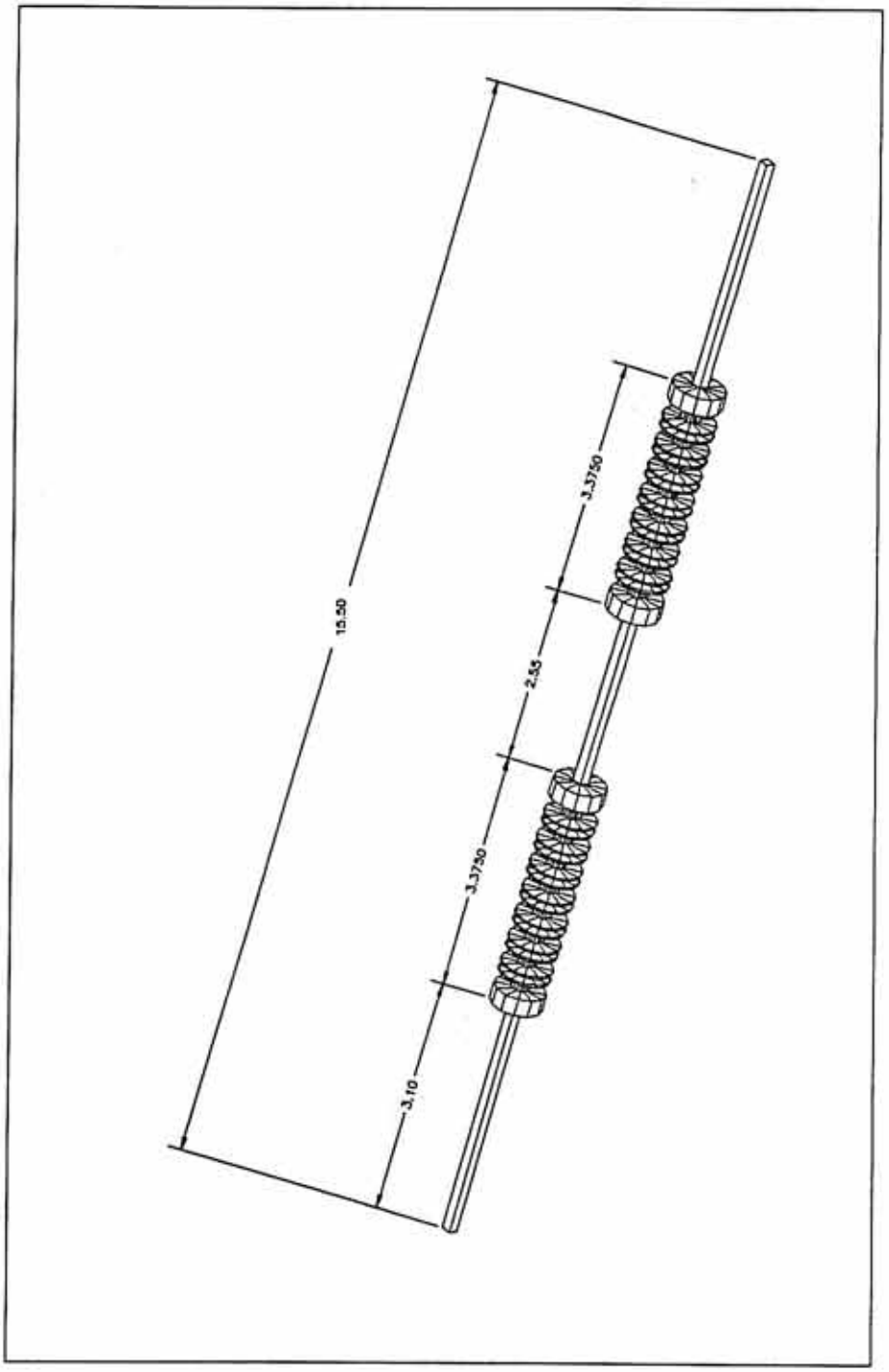
15.50
3.3750
2.55
3.3750
3.10

Figure 8. A sketch of the Polar and Wind search coil bobbins. Dimensions are given in inches.

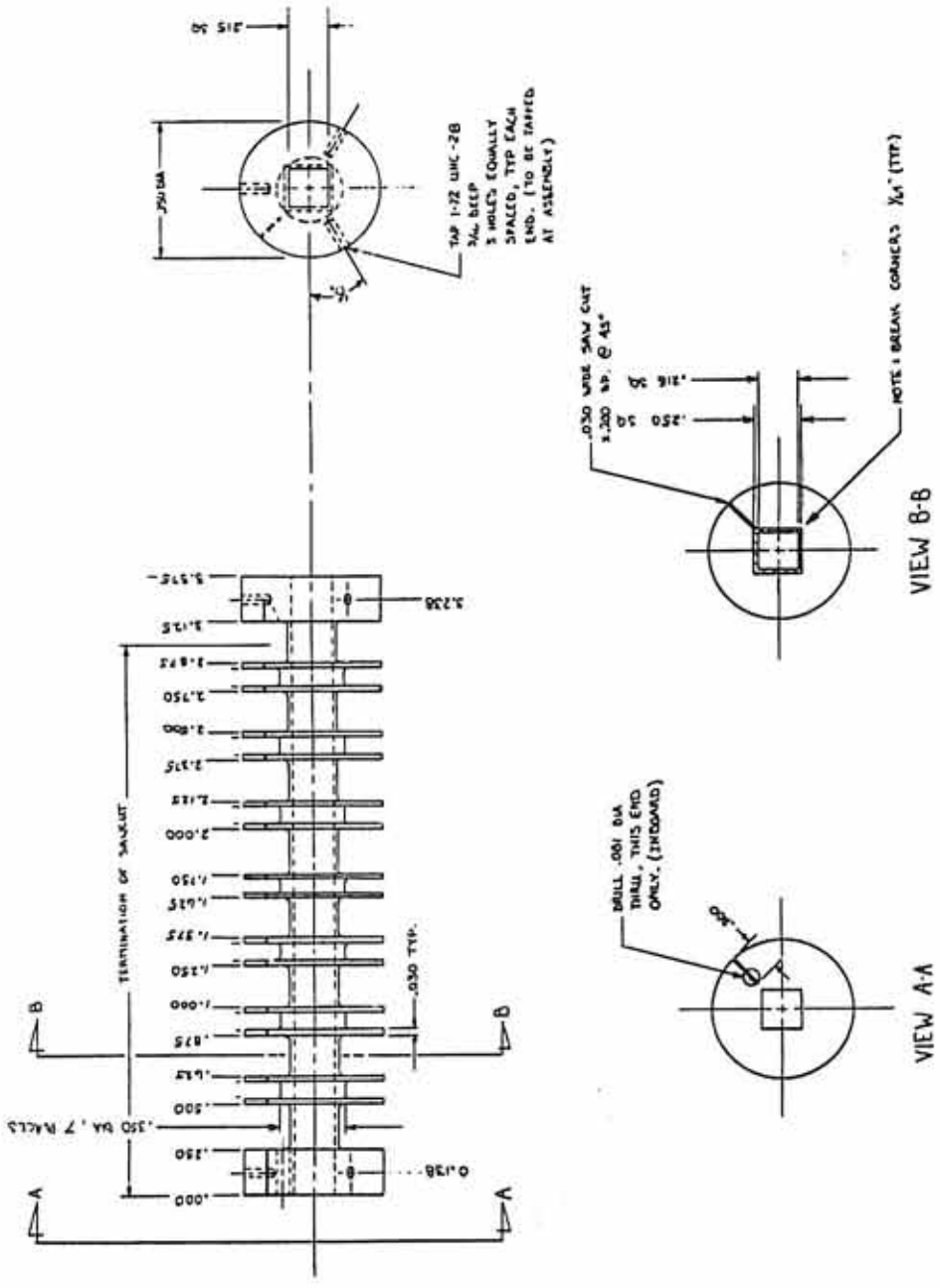
TAP 1-72 UNC-2B
3/4" DEEP
3 HOLES EQUALLY
SPACED, TYP EACH
END. (TO BE TAPED
AT ASLEMBLY)
TERMINATION OF SAWCUT
.350 DIA, 7 PLCS
.050 TYP.
.030 WIDE SAW CUT
±.200 DP @ 45°
NOTE: BREAK CORNERS 1/64" (TYP)
VIEW B-B
DRILL .001 DIA
THRU, THIS END
ONLY. (INBOARD)
VIEW A-A

Figure 9. A sketch of the Polar and Wind search coil bobbins. The primary windings are located in sections 1 through 7. The calibration winding is located in section 8.

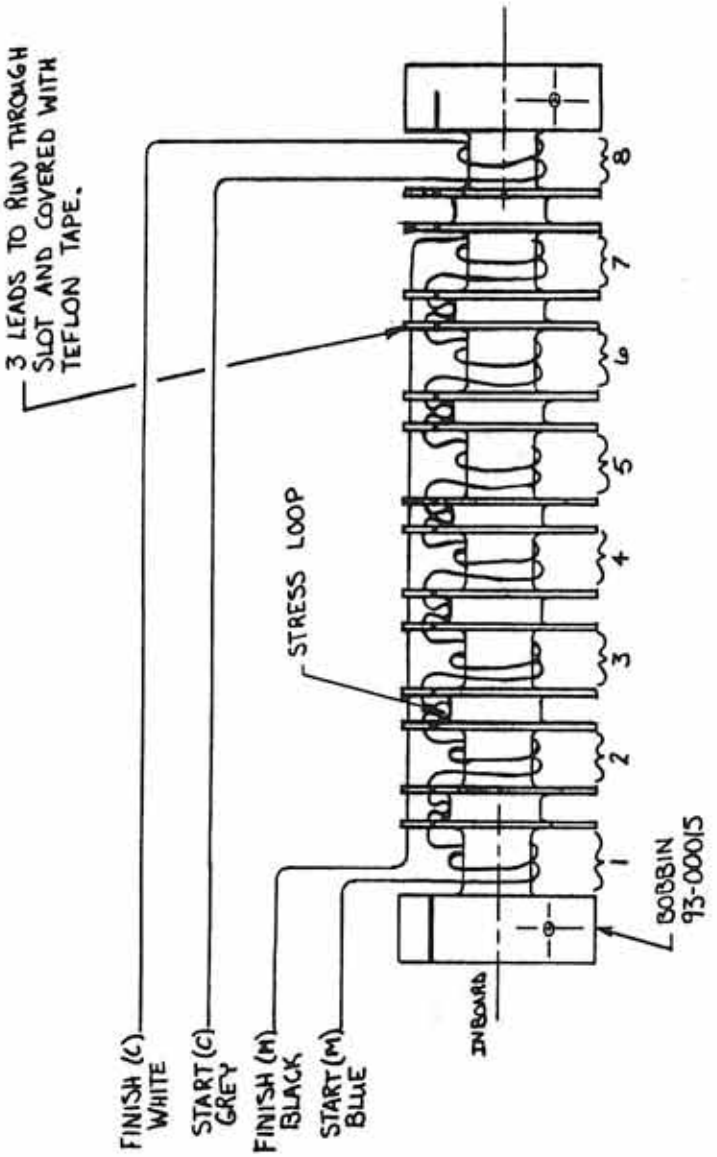
3 LEADS TO RUN THROUGH SLOT AND COVERED WITH TEFLON TAPE.
STRESS LOOP
FINISH (C) WHITE
START (C) GREY
FINISH (M) BLACK
START (M) BLUE
IN BOARD
BOBBIN 93-00015
1
2
3
4
5
6
7
8

Figure 10. The relationship of the effective permeability determined from the position of the bobbins on the core to the output voltage of the preamplifier as measured on the Polar engineering model search coil.

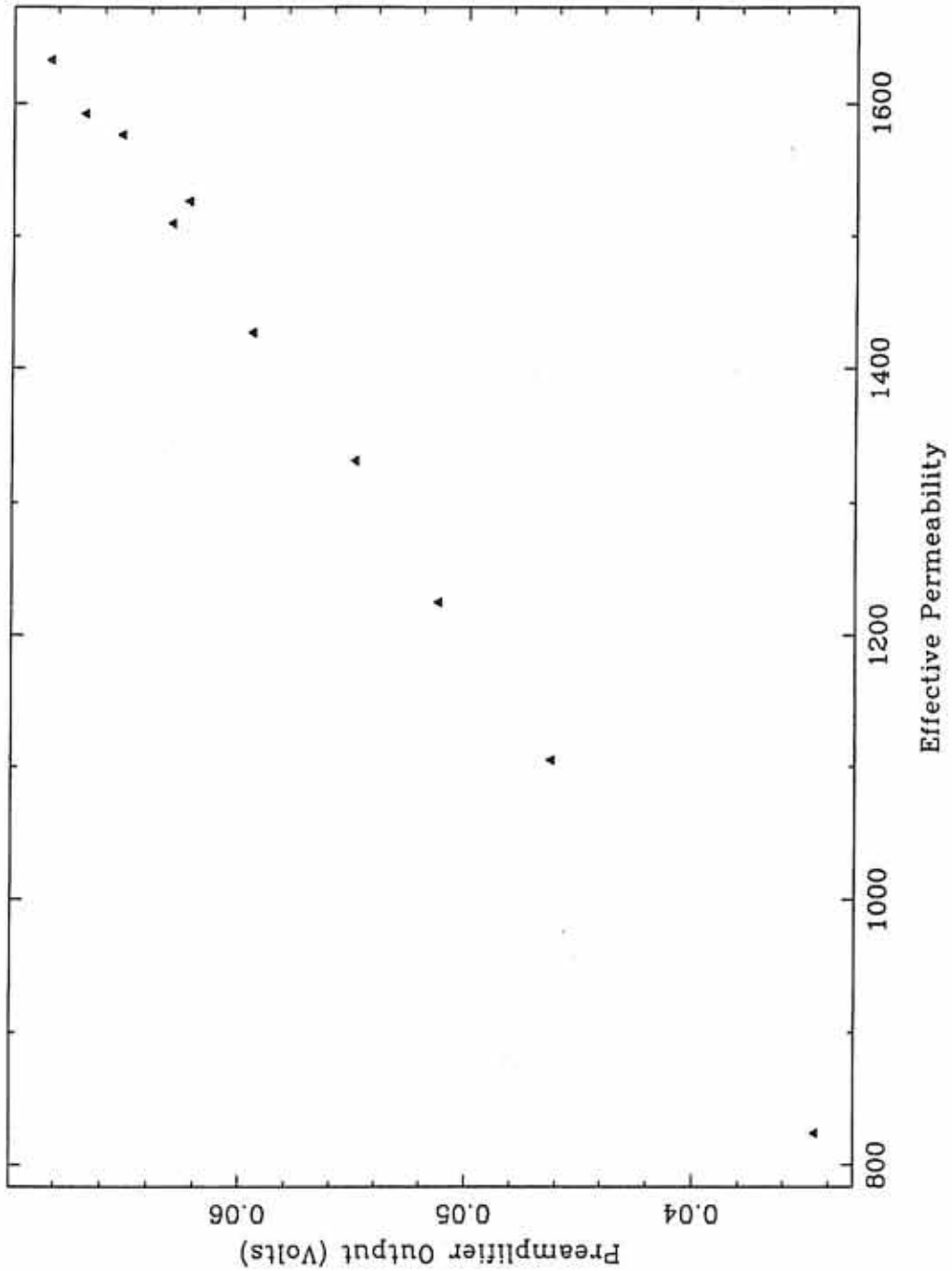
Preamplifier Output (Volts)
0.04
0.05
0.06
800
1000
1200
1400
1600
Effective Permeability

Figure 11. The relationship of the effective permeability determined from the position of the bobbins on the core to the inductance of the coils as measured on the Polar engineering model search coil. The inductance of bobbin 1 is represented by the circles and bobbin 2 by the squares.

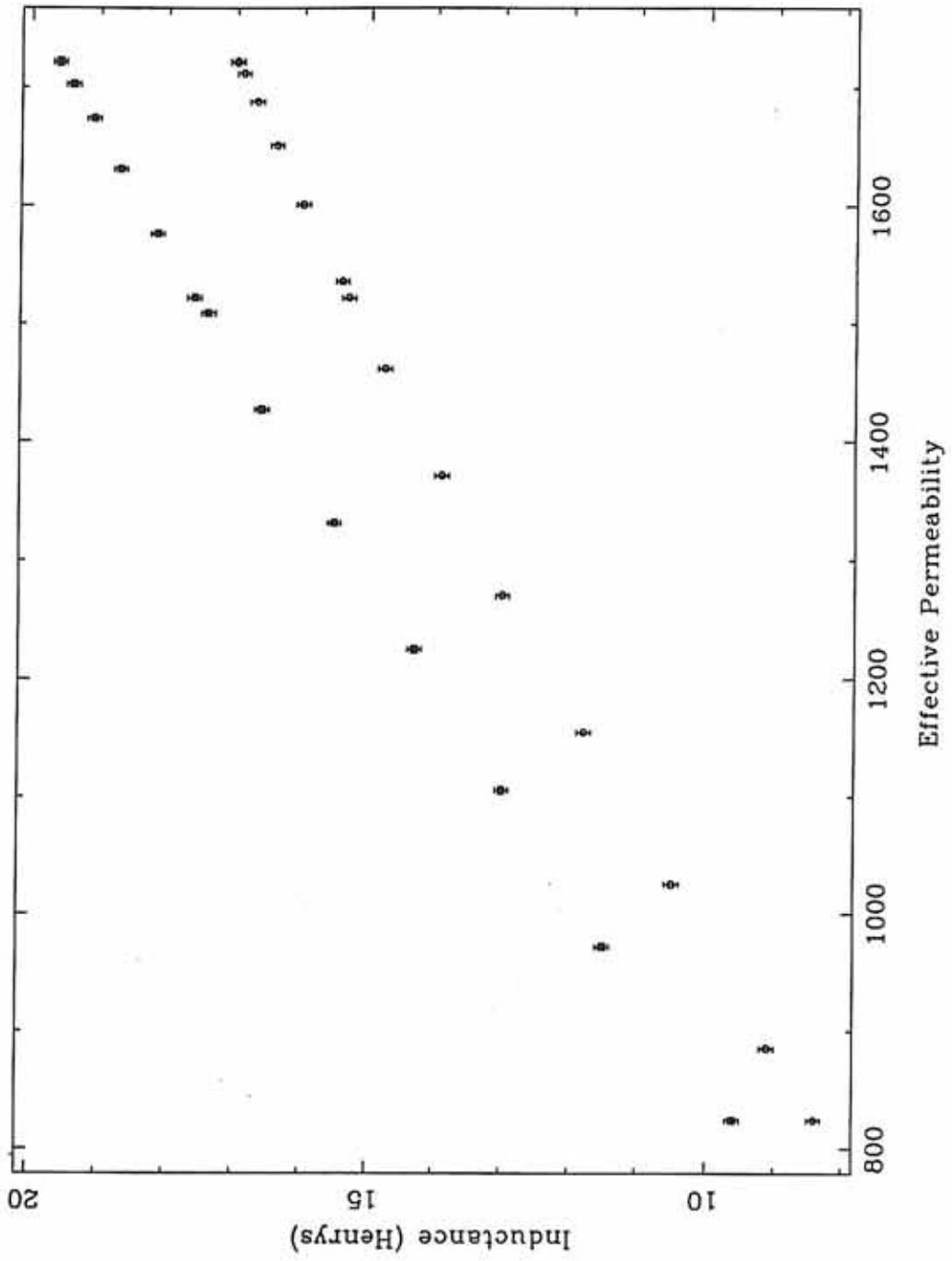
Inductance (Henrys)
20
15
10
800
1000
1200
1400
1600
Effective Permeability

Figure 12. A schematic of the Polar search coil preamplifier. The Wind search coil preamplifier is identical except for resistors R2 and R26, which have a value of 1 M ohm.

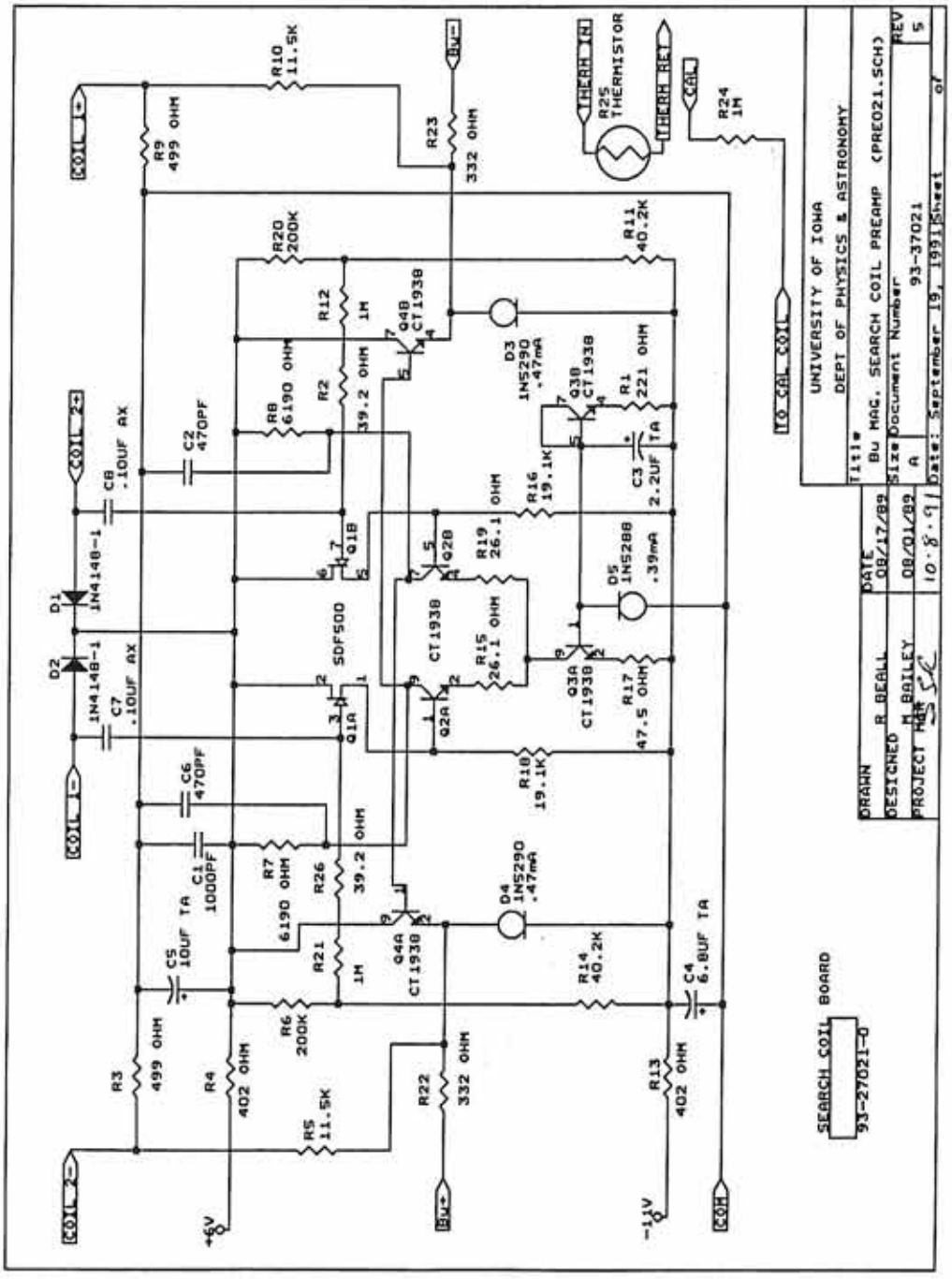
COIL 1+
COIL 2+
COIL 1-
COIL 2-
R10 11.5K
R9 499 OHM
R23 332 OHM
+6V
BW+
-11V
COM
THERM IN
THERM RET
CAL
R25 THERMISTOR
R24 1M
TO CAL COIL
R20 200K
R11 40.2K
R12 1M
Q4B CT1938
R8 6190 OHM
R2 39.2 OHM
C2 470PF
C8 .10UF AX
D3 IN5290 .47mA
Q3B CT1938
R1 221 OHM
C3 2.2UF TA
D1 IN4148-1
R16 19.1K
Q1B
Q2B
R19 26.1 OHM
D5 IN5288 .39mA
D2 IN4148-1
C7 .10UF AX
SDF500
Q1A
CT1938
R15 26.1 OHM
Q3A CT1938
R17 47.5 OHM
Q2A
C6 470PF
R18 19.1K
C1 1000PF
R7 6190 OHM
R26 39.2 OHM
D4 IN5290 .47mA
C5 10UF TA
R21 1M
Q4A CT1938
R14 40.2K
C4 6.8UF TA
R3 499 OHM
R4 402 OHM
R6 200K
R22 332 OHM
R13 402 OHM
R5 11.5K
SEARCH COIL BOARD
93-27021-0
UNIVERSITY OF IOWA
DEPT OF PHYSICS & ASTRONOMY
Title
Bu MAG. SEARCH COIL PREAMP (PRE021.SCH)
Size
A
Document Number
93-37021
REV
S
Date: September 19, 1991 Sheet of
DRAWN R BEALL 08/17/89
DESIGNED M BAILEY 08/01/89
PROJECT MGR 10·8·91

Figure 13. A block diagram of the Polar and Wind search coil preamplifier.

A-G92-122

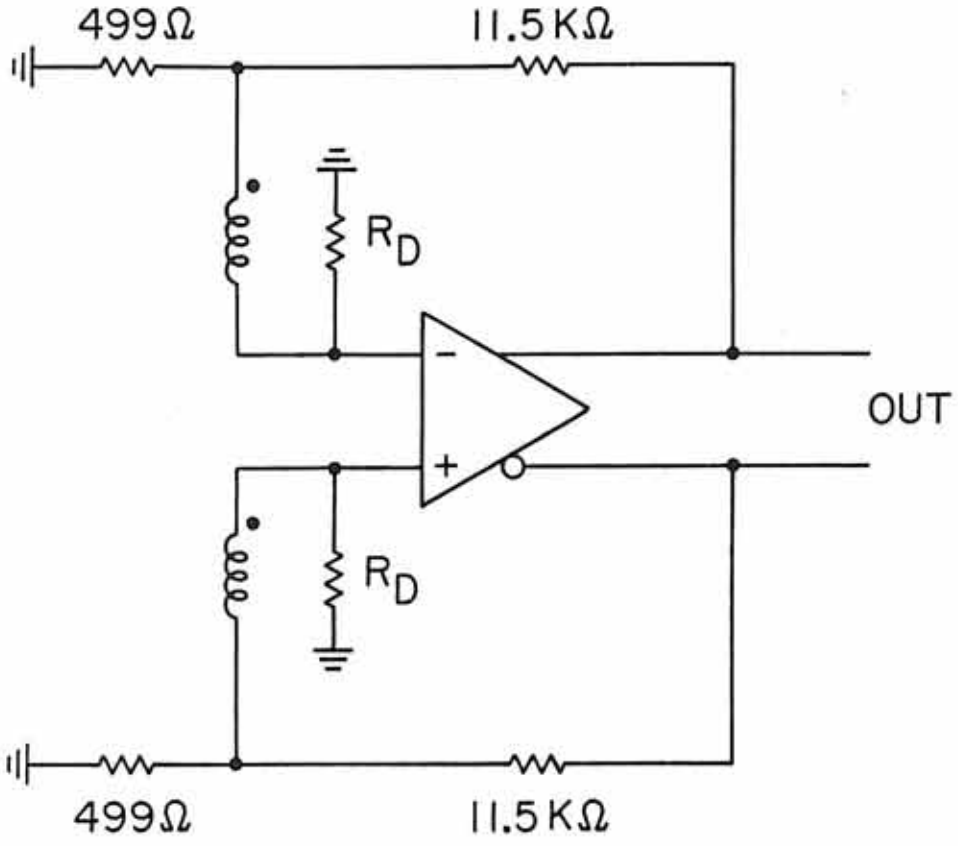

Figure 14. A block diagram of the Polar and Wind search coil preamplifier when a differential signal is applied at the inputs.

A-G92-121

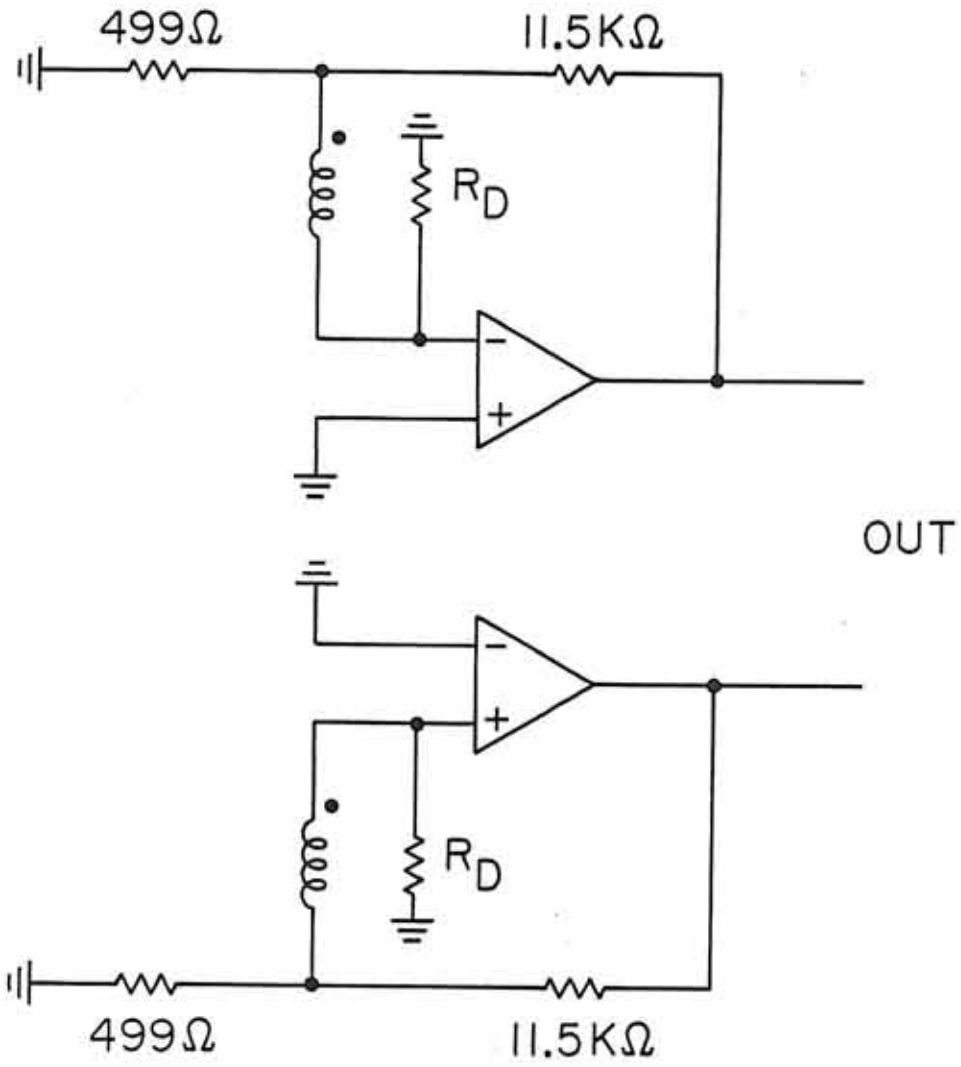

Figure 15. The transfer function of the Polar prototype model search coil (circles) compared to the theoretical prediction (solid line) from Equation 7.

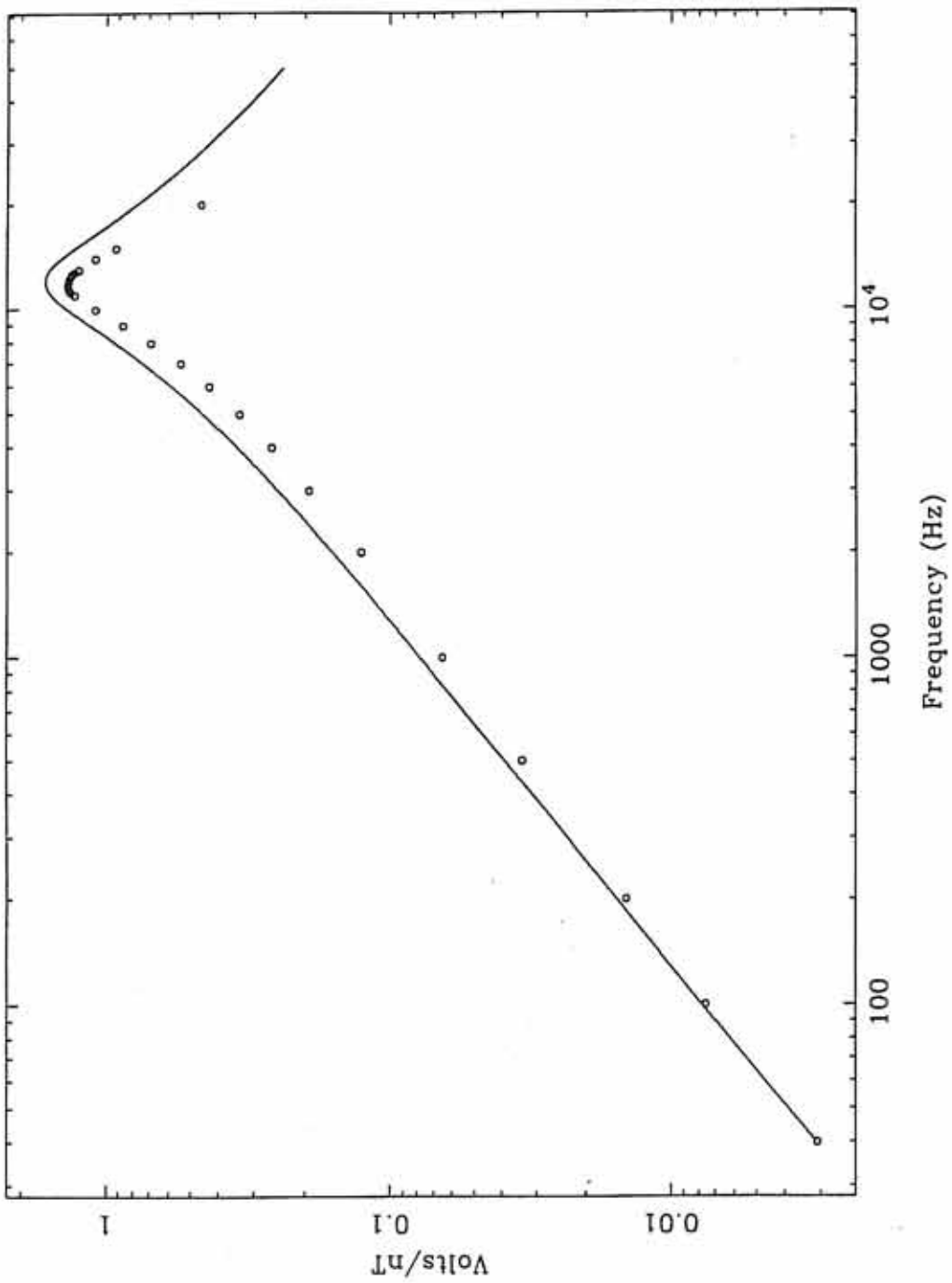
Volts/nT
0.01
0.1
1
100
1000
10^4
Frequency (Hz)

Figure 16. A comparison of the Polar prototype model search coil noise level (squares) with the ISEE 1 and 2 search coil noise levels (solid lines).

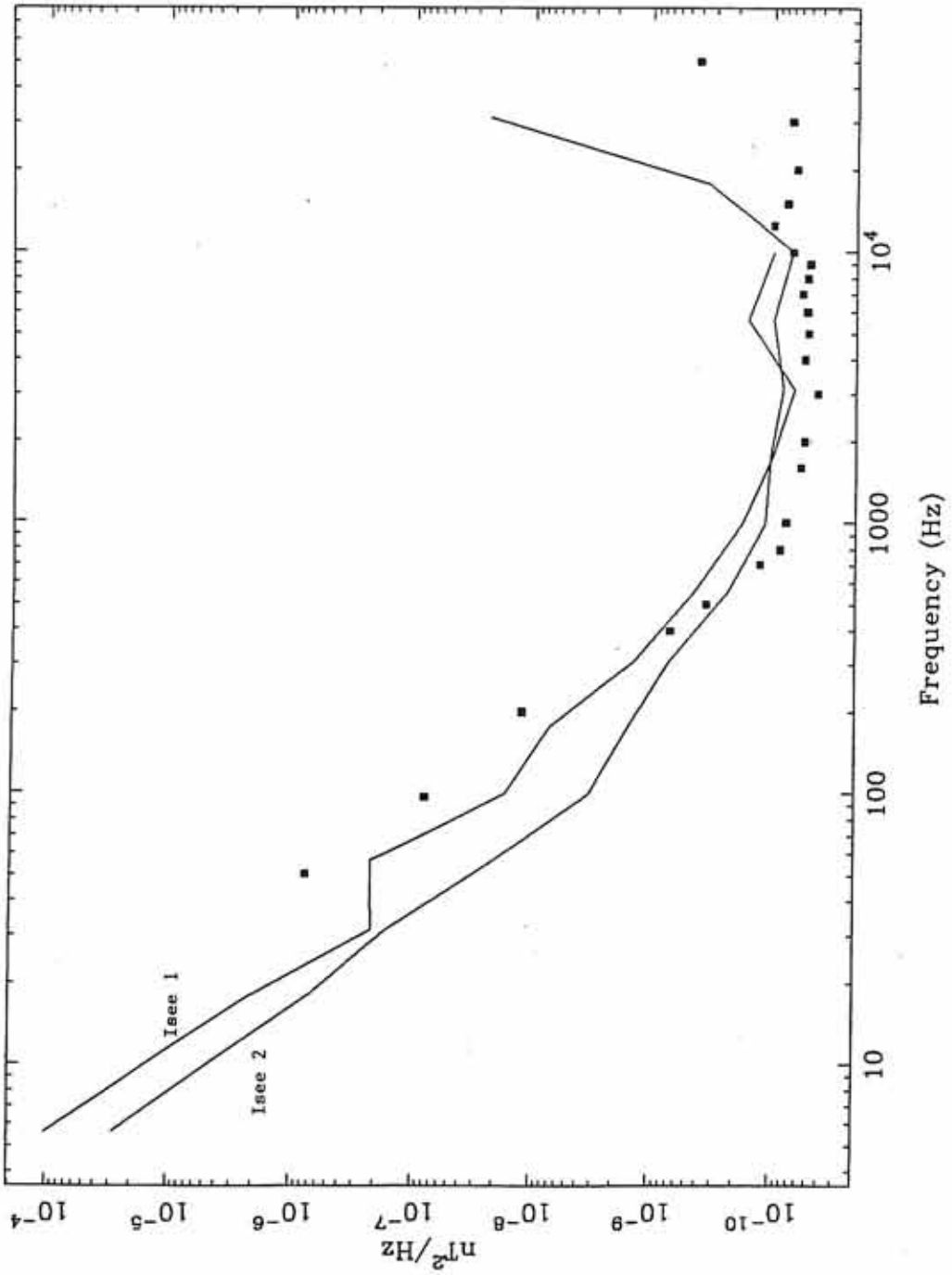
Isee 1
Isee 2
nT^2/Hz
10^{-4}
10^{-5}
10^{-6}
10^{-7}
10^{-8}
10^{-9}
10^{-10}
10
100
1000
10^4
Frequency (Hz)

Figure 17. The transfer function of the Wind spare search coil (circles) compared to the theoretical prediction (solid line) from Equation 7.

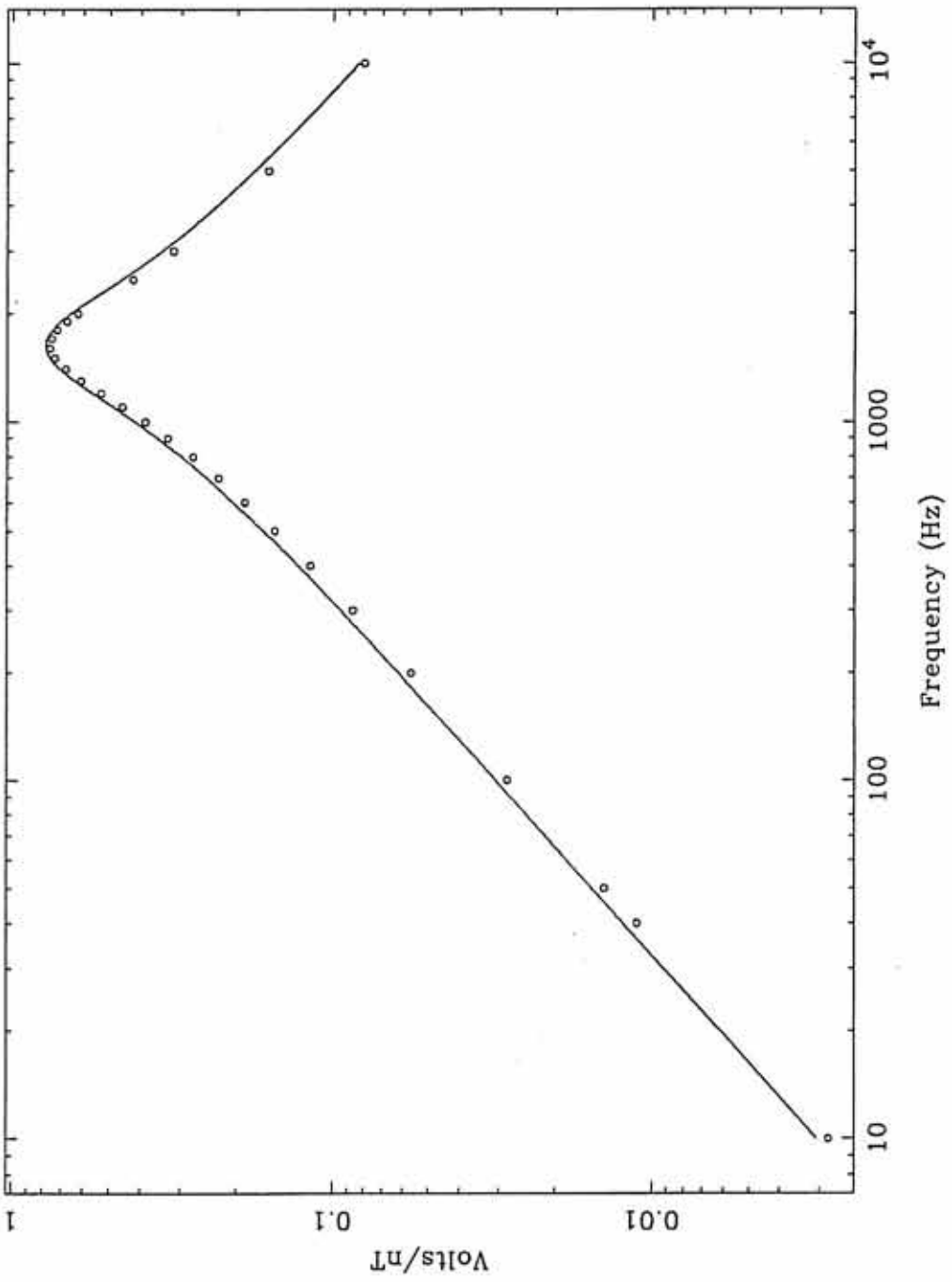
Volts/nT
1
0.1
0.01
10
100
1000
10^4
Frequency (Hz)

Figure 18. A comparison of the Wind spare search coil noise level (squares) with the ISEE 3 search coil noise levels (solid line).

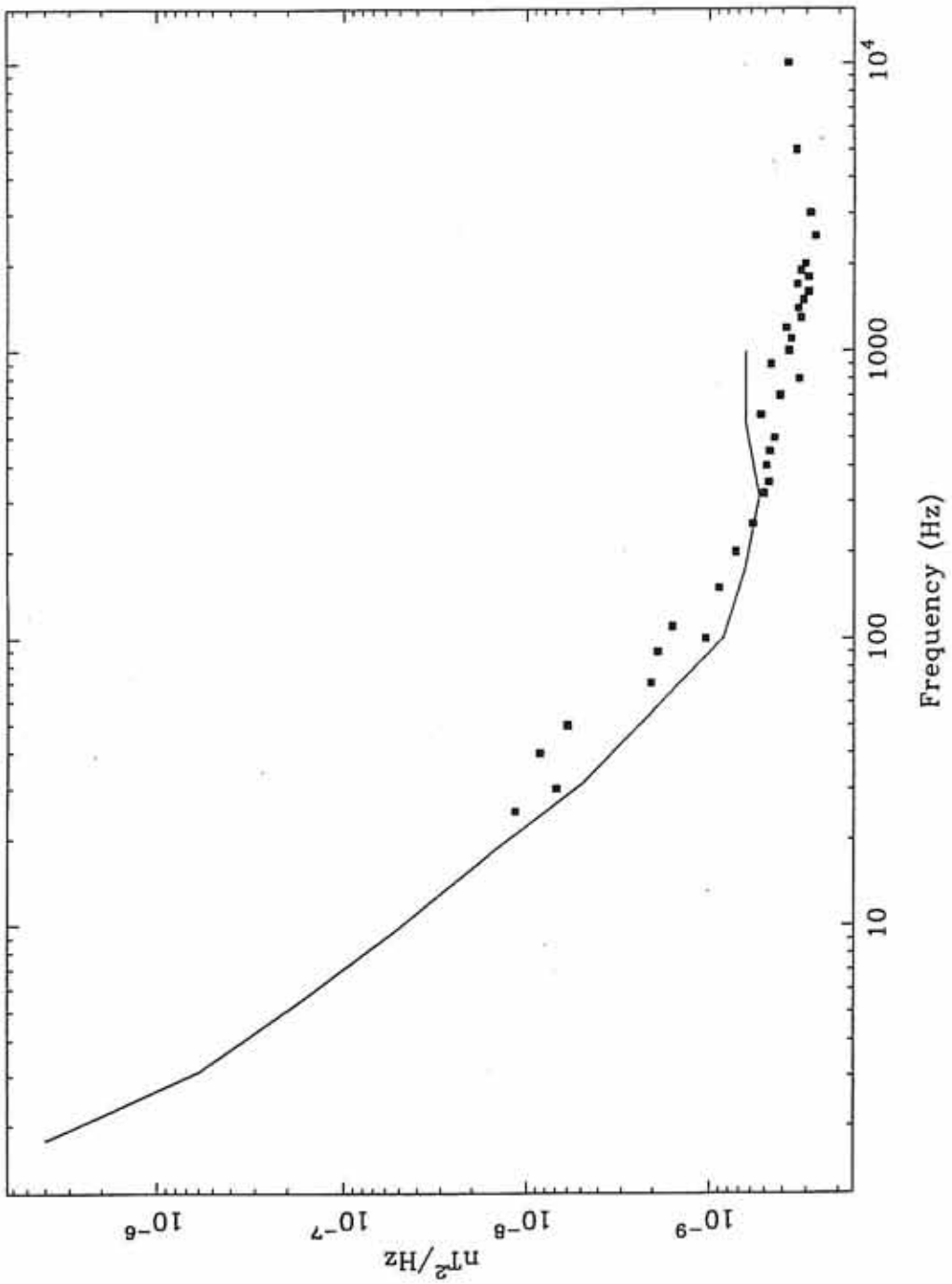
nT²/Hz
10⁻⁹
10⁻⁸
10⁻⁷
10⁻⁶
10
100
1000
10⁴
Frequency (Hz)

Figure 19. A photograph of the Wind B_z search coil magnetometer.

Magnetic Search Coils
GGS WIND - WAVES
The University of Iowa

BW-Z

Figure 20. A sketch of a typical setup of the transmitting loop calibration method.

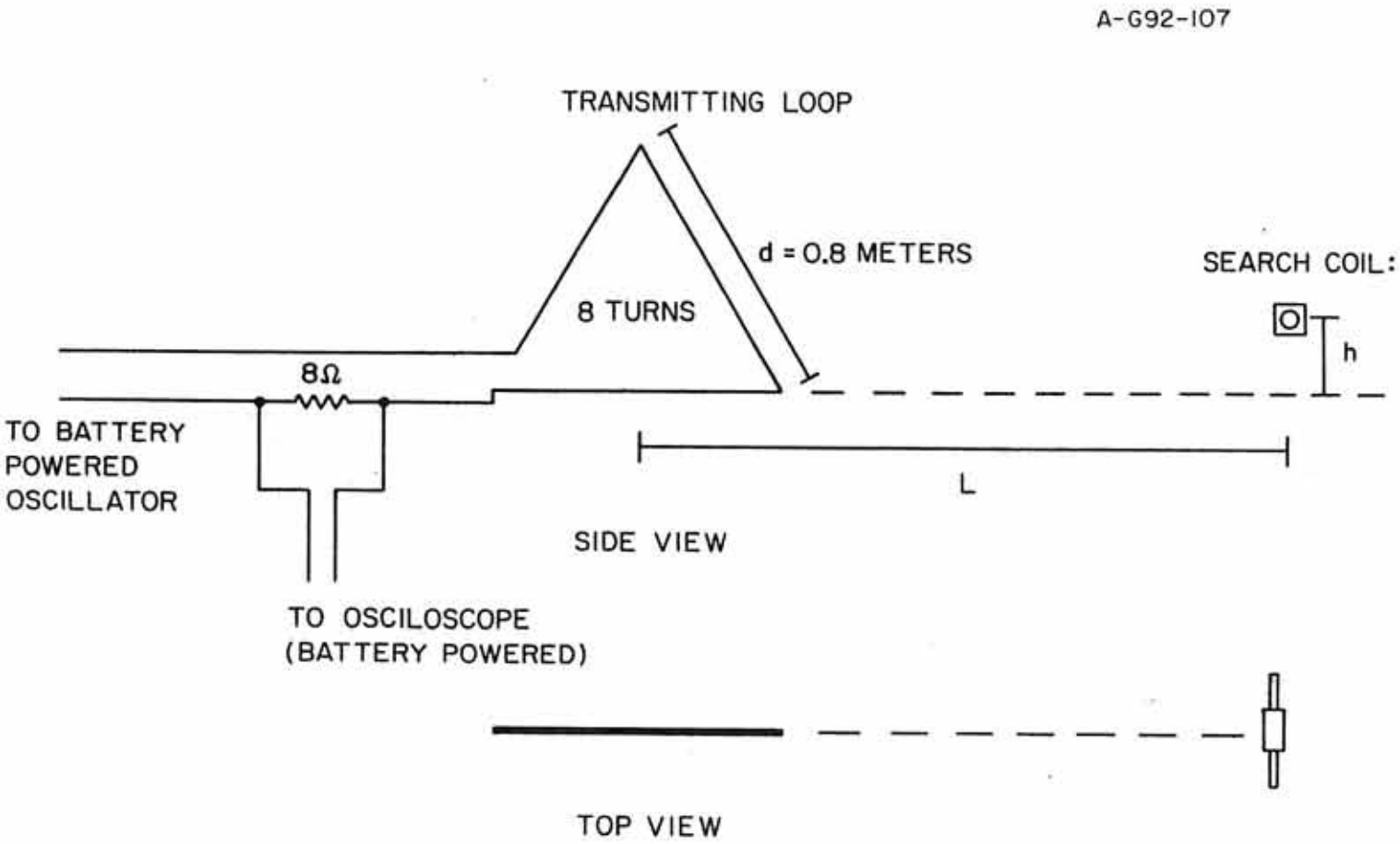
A-G92-107
TRANSMITTING LOOP
d = 0.8 METERS
SEARCH COIL:
8 TURNS
h
8Ω
TO BATTERY
POWERED
OSCILLATOR
L
SIDE VIEW
TO OSCILOSCOPE
(BATTERY POWERED)
TOP VIEW

Figure 21. A comparison of the coil constant determined by the transmitting loop method in the lab at L = 5 feet (squares) and L = 8 feet (circles). The difference of the curves is probably due to the steel beams in the floor and ceiling distorting the calibration signal.

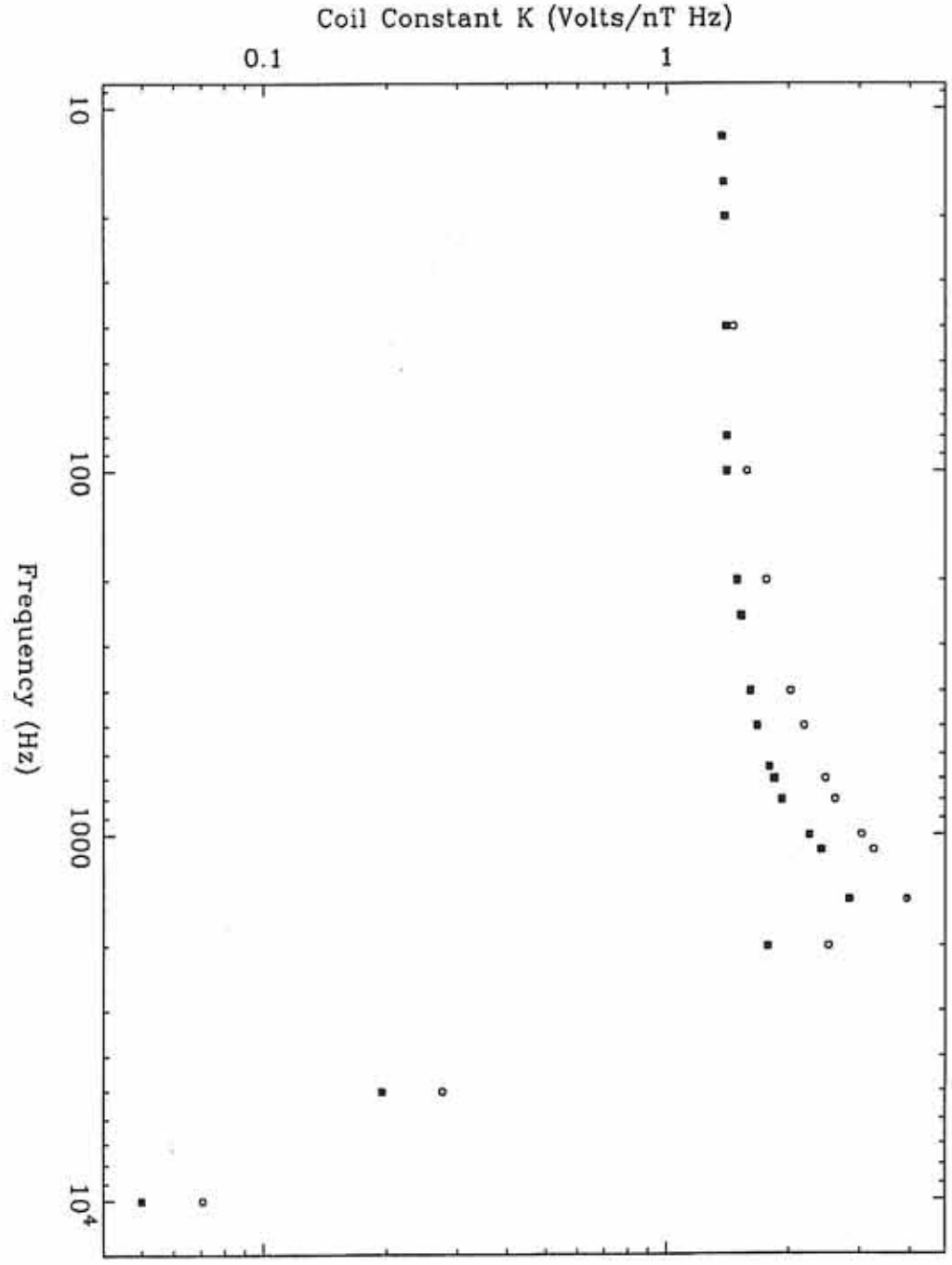
Coil Constant K (Volts/nT Hz)
0.1
1
10
100
1000
10^4
Frequency (Hz)

Figure 22. The equivalent circuit of the solenoid used to calibrate the search coil magnetometers.

A-G92-119

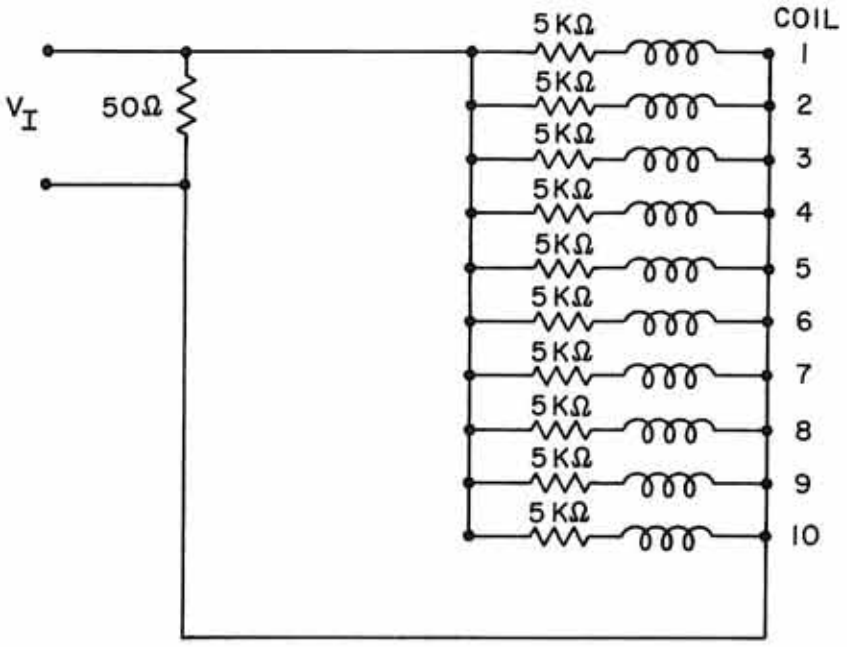
5KΩ
COIL
1
5KΩ
2
5KΩ
3
5KΩ
4
5KΩ
5
5KΩ
6
5KΩ
7
5KΩ
8
5KΩ
9
5KΩ
10
V_I
50Ω

Figure 23. A comparison of the transfer function of the Wind spare search coil magnetometer determined by the solenoid in the μ-metal shield and the transmitting loop method at L = 5 feet and L = 8 feet. The circles are the μ-metal shield method. The triangles are the transmitting loop method at L = 5 feet, and the squares are L = 8 feet.

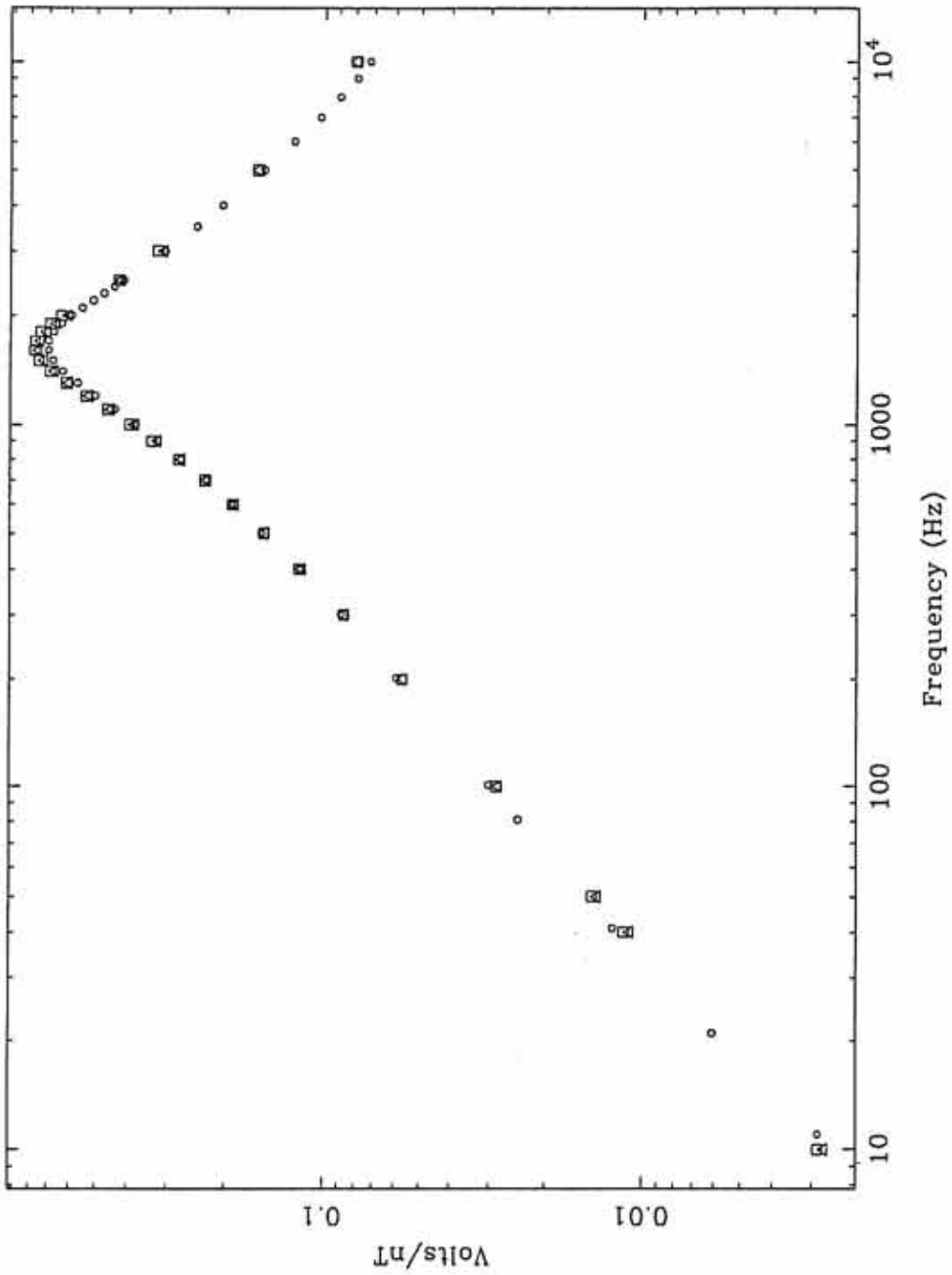
Volts/nT
0.1
0.01
10
100
1000
10^4
Frequency (Hz)

Figure 24. A sketch of the setup for the noise voltage calibration. The search coil magnetometer is placed in a μ-metal shield and powered by batteries. The noise voltage is measured by a spectrum analyzer.

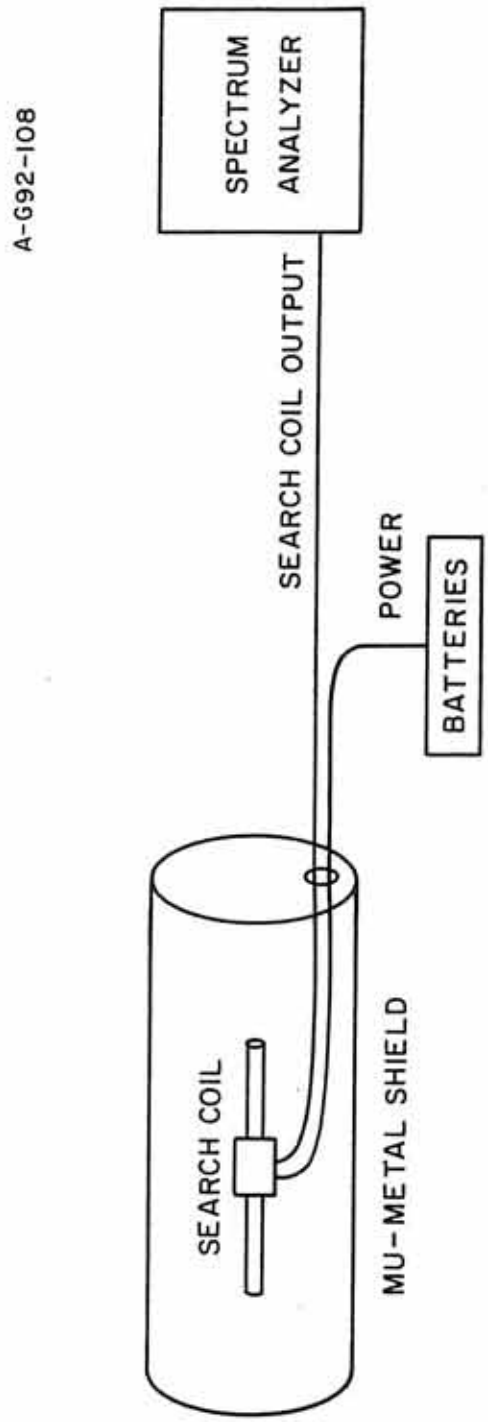
A-692-108
SPECTRUM ANALYZER
SEARCH COIL OUTPUT
POWER
BATTERIES
SEARCH COIL
MU-METAL SHIELD

Figure 25. A comparison of the Wind search coil noise level determined in the lab (circles) and at a low noise field site (squares).

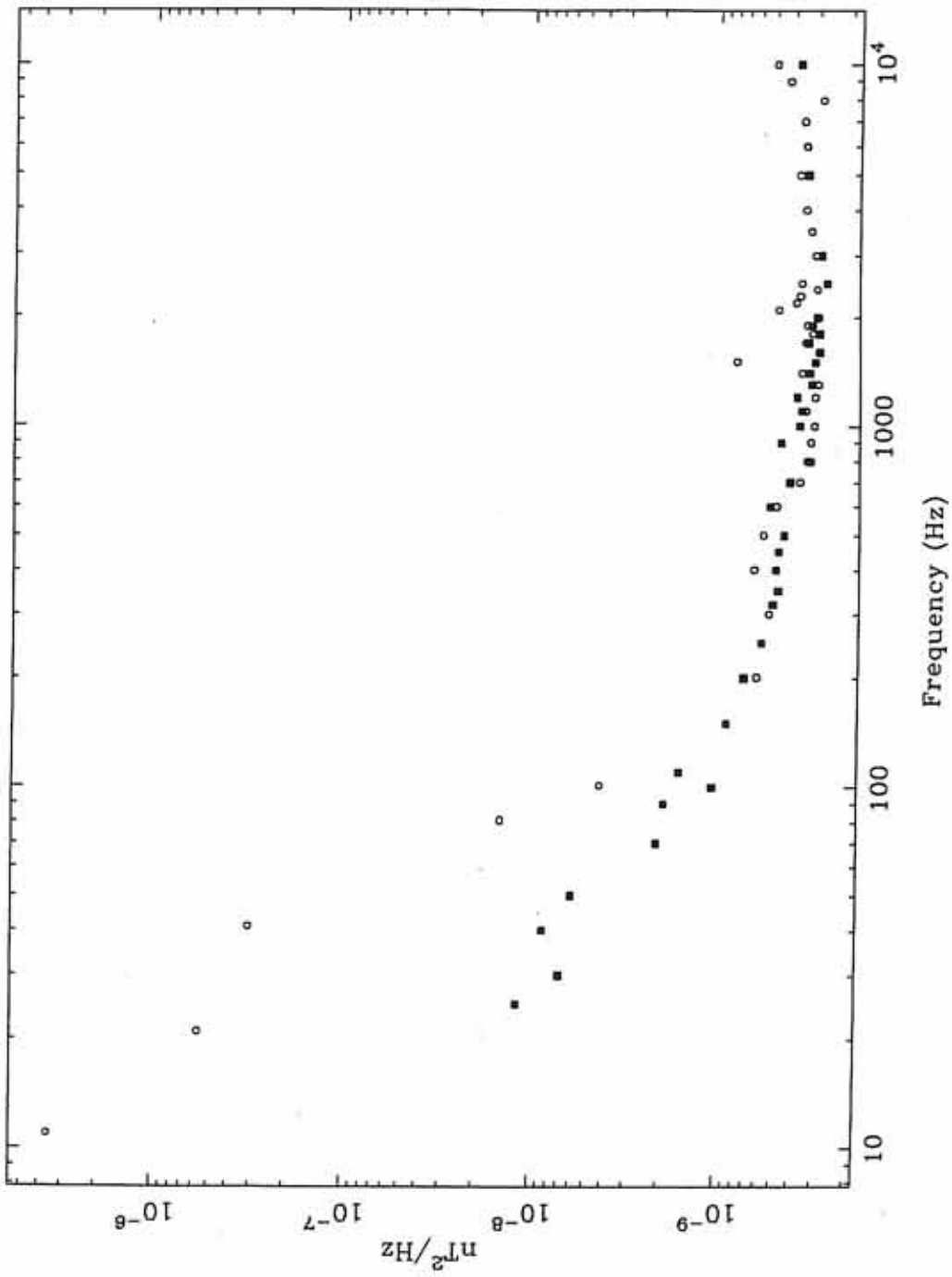
nT^2/Hz
10^{-6}
10^{-7}
10^{-8}
10^{-9}
10
100
1000
10^4
Frequency (Hz)

Figure 26. A sketch of the negative feedback system used on the Japanese Geotail search coil. A winding of two turns provides the negative feedback.

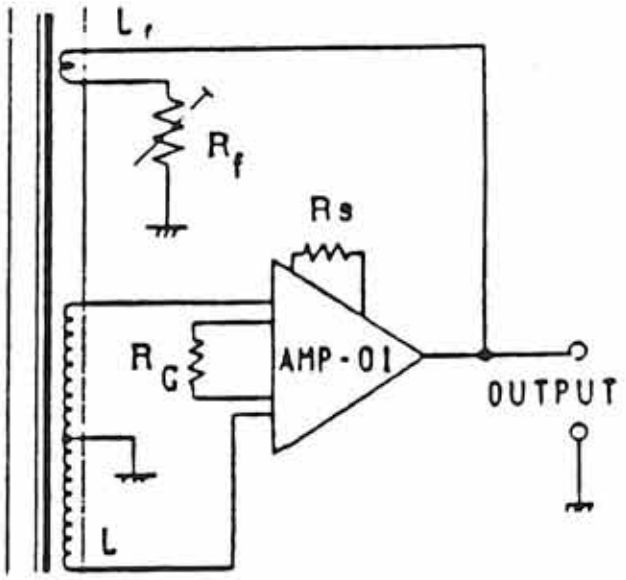
L_f
R_f
Rs
R_G
AMP-01
OUTPUT
L